

**Niger Delta gravity-driven deformation above the relict Chain and
Charcot oceanic fracture zones, Gulf of Guinea: insights from analogue
models**

Jonny E. Wu^{*1,2}, Ken McClay¹, Edyta Frankowicz^{1,3}

*Corresponding author

¹Fault Dynamics Research Group, Royal Holloway, University of London,
Egham, Surrey, TW20 0EX

²Now at: Department of Geosciences, National Taiwan University, Taipei City,
10617, Taiwan. jonnywu@ntu.edu.tw

³Now at: Shell International Exploration & Production, The Hague,
Netherlands

Keywords: deltas, overpressured shales, gravity-driven deformation, Niger
Delta, oceanic fracture zones, analogue modelling, basement steps

Abstract

The Niger Delta is a classic example of a passive margin delta that has
gravitationally deformed above an overpressured shale decollement. The
outboard Niger Delta clastic wedge, including the Akata Formation
overpressured shale decollement, is differentially thickened across relict
oceanic basement steps formed at the Chain and Charcot fracture zones. In
this study, five analogue models were applied to investigate the effects of a

differentially thickened overpressured shale decollement across relict stepped basement on Niger Delta gravity-driven deformation. Gravity-driven delta deformation was simulated by allowing a lobate, layered sandpack to deform by gravity above a ductile polymer. A first series of experiments had a featureless, horizontal basement whereas a second series had differentially thickened polymer above Niger Delta-like basement steps. Two syn-kinematic sedimentation patterns were also tested. Surface strains were analysed using digital image correlation and key models were reconstructed in 3D. All five model deltas spread radially outward and formed arcuate delta top grabens and arcuate delta toe folds. The arcuate structures were cut by dip-oriented radial grabens and delta toe oblique extensional tear faults. The basement steps models formed dual, divergent spreading directions that had perturbed updip delta top growth faults. Similarities between the analogue model structures and the Niger Delta strongly suggest that the lobate Niger Delta top has spread radially outward. The basement step models indicate the potential for partitioned Niger Delta gravity spreading across the Chain and Charcot fracture zones basement steps due to a thicker or more highly overpressured Akata Fm. shale detachment. Faster gravity spreading north of the Charcot fracture zone has potentially contributed to the Niger Delta toe 'dual lobe' geometry and influenced Niger Delta top growth fault patterns, and implies that the Niger Delta western lobe toe thrusts have been very active.

1. Introduction

The Niger Delta has prolific hydrocarbon reserves and is a well-documented example of gravity-driven deformation at a passive margin delta above an overpressured shale detachment (Fig. 1) (Doust and Omatsola, 1990; Haack et al, 2000; Corredor et al., 2005; Cobbold et al., 2009). The Niger Delta clastic wedge is up to 12 km thick and has a concave-seaward, lobate profile in plan view (Fig. 1b) (Cobbold et al., 2009). The main deltaic sedimentation pulse began in the Eocene and the delta front has prograded outward approximately 300 km to its present-day position (Evamy et al., 1978). Gravity-driven deformation is characterized by delta top extensional faults and delta toe imbricate fold-thrusts that detach within the Akata Formation, a prodelta marine shale that is typically overpressured (Figs. 1c & d). Deformation began in the Eocene and continues to the present-day (Doust and Omatsola, 1990; Cobbold et al., 2009).

The outboard Niger Delta has gravitationally deformed above stepped oceanic basement formed by the Chain and Charcot fracture zones (Figs. 1a & b). The fracture zones were transforms during mid-Atlantic opening in the Aptian and have been inactive since the Santonian (Lehner and de Ruiter, 1977; Briggs et al., 2009). Geodynamic models show that fossil transforms juxtapose oceanic lithosphere of different ages that thermally subside at different rates, producing differential sediment thickening across the transform (Sibuet and Mascle, 1978). This appears to be true at the Niger Delta, where regional isopach maps show differential thickening of the Niger Delta clastic

1 wedge across the fossil fracture zones (Figs. 1a & b) (.cf MacGregor et al.,
2 2003; Cobbold et et al., 2009). This has implications for the Akata Formation
3 overpressured shale decollement, which is seen in seismic profiles to thicken
4 and onlap across the fracture zones (see Figure 3 of Morgan, 2004).
5
6 Thickening of the overpressured shale decollement across the stepped
7 basement may have affected Niger Delta gravity-driven deformation but has
8 not been fully evaluated.
9

10
11
12
13
14
15
16
17
18
19 3D seismic studies have also beautifully illustrated the localised high
20 basement relief along the fracture zones, including 1.4 km-high buried
21 volcanoes near the Chain Fracture Zone landward termination (Davies et al.,
22 2005). Other studies have shown an elongate, ~7 km-high, buried basement
23 ridge across the Charcot Fracture Zone, outboard of the Niger Delta
24 deformation front (Davies et al., 2005; Briggs et al., 2009). It is quite probable
25 that these local basement structures have likely played some role in
26 buttressing or localising strains at the Niger Delta toe thrust belt. For
27 example, tear faults and segmented thrusts have formed above the Chain
28 Fracture Zone volcanoes (Morgan, 2003; 2004). Many have also noted that
29 the prominent separation between the Niger delta toe thrust lobes above the
30 Charcot Fracture Zone (Fig. 1c) (e.g. Cobbold et al., 2009).
31
32
33
34
35
36
37
38
39
40
41
42
43
44
45
46
47
48
49
50

51 In this study dry sand and silicone polymer analogue models were applied to
52 investigate the effects of relict oceanic fracture zone stepped basement on
53 Niger Delta gravity-driven deformation, focusing on the potential effects of a
54 differentially thickened overpressured shale decollement. Sand-silicone
55
56
57
58
59
60
61
62
63
64
65

analogue models are a well-documented technique for modelling gravity-driven delta systems (e.g. Cobbold and Szatmari, 1991). The models allow deformation to be driven simply by the gravity potential of the initial delta load and applied syn-kinematic sedimentation patterns (e.g. Cobbold and Szatmari, 1991; Ge et al., 1997; McClay et al., 1998; Vendeville et al., 2005). Basement topographies and distal buttresses have been tested as boundary parameters (e.g. Loncke et al., 2010; Sellier et al., 2013). Published studies using this modelling technique have reproduced many typical gravity-driven delta strain patterns including linked proximal extensional and distal compressional systems and spoke-like, radial extensional grabens (e.g. Cobbold and Szatmari, 1991; McClay et al., 1998; Gaullier and Vendeville, 2005). Other published studies have contributed important insights to gravity-driven deformation across specific basement features at the offshore Nile fan and the Florence Rise, offshore Cyprus (Loncke et al., 2010; Sellier et al., 2013).

Here we present five 3D sand and silicone polymer analogue models that tested two parameters on gravity-driven deformation of a model lobate delta: (1) basement steps – a featureless, horizontal basement; and a Niger Delta-like stepped basement that partitioned a differentially thickened pre-deformation basal polymer; and, (2) syn-kinematic sedimentation styles – aggradational and progradational (Table 1 & Figs. 2, 3 & 4). The two syn-kinematic sedimentation patterns allowed the basement configurations to be tested against a range of differential loading patterns.

1 Deformation was closely monitored using digital image correlation (DIC) (e.g.
2 Adam et al., 2005). Key models were digitally reconstructed to visualize
3
4 internal geometries in 3D. Fault patterns were interpreted from plan view and
5
6 cross-sectional photographs. In this study we emphasize the regional-scale
7
8 structural zonations in the models – and limit the analysis of individual
9
10 structures – as the sand-silicone analogue models have well-known
11
12 limitations that do not permit a full range of structural styles to be reproduced
13
14 when used as a proxy for overpressured shales. The limited range of
15
16 structural styles is particularly evident at the model delta toe, where polymer-
17
18 cored detachment fold styles are typically produced (e.g. McClay et al., 1998).
19
20 These structural styles more closely resemble other deltas above salt, or
21
22 other deltas with overpressured shale substrates such as the offshore western
23
24 Gulf of Mexico (e.g. Rowan et al., 2004; Alzaga-Ruiz et al., 2009). Based on
25
26 the model results, we show in this paper the following potential effects of
27
28 differentially thickened overpressured shales across the Chain and Charcot
29
30 oceanic basement fracture zones: (1) partitioning of radial outward gravity
31
32 spreading into two main divergent directions at the Niger delta toe, providing a
33
34 potential contributing factor for the dual lobe geometry, (2) localised oblique
35
36 extensional strains above the basement steps, and (3) perturbed updip Niger
37
38 delta top growth faults.
39
40
41
42
43
44
45
46
47
48
49
50

51 **2. Experimental method**

52
53
54
55

56 In all models a basal SGM36 silicone polymer layer simulated an
57
58 overpressured shale substrate (Fig. 2a). A 4-6 mm uniform layer of dry quartz
59
60
61
62
63
64
65

1 sand was mechanically sieved above the basal polymer layer to form a pre-
2 kinematic sequence (Fig. 2c). A 20 mm-thick delta lobe of layered dry quartz
3 sand was mechanically sieved to form a pre-kinematic differential load (Fig.
4 2a). Pre-kinematic sand layers were coloured blue or green, white, and black
5 (Fig. 2c). The lobate delta load was allowed to passively deform by gravity
6 above the basal polymer layer over a period of up to 14.5 hours (Table 1).
7
8
9
10
11
12
13
14
15

16 *2.1 Syn-kinematic sedimentation*

17
18
19
20

21 During deformation syn-kinematic sedimentation was infilled at regular time
22 intervals (see Fig. 2b, Fig 4 & Table 1). The syn-kinematic sand layers
23 alternated between red, white, and black colours (Fig. 2c). The half-hour to
24 hourly frequency of the syn-kinematic sedimentation events was sufficient to
25 minimise emergent polymer structures (e.g. diapirs, overhangs, and nappes)
26 that are more characteristic of gravity-driven deltas above salt.
27
28
29
30
31
32
33
34
35
36
37
38

39 Models 1 & 4 had aggradational syn-kinematic sedimentation on the delta top
40 only, whereas Models 2, 3 & 5 had progradational syn-kinematic
41 sedimentation on both the delta top and delta toe (Figure 4 & Table 1). Delta
42 top sedimentation was performed by infilling the delta top grabens and
43 mechanically sieving a 3-4 mm-thick layer of dry quartz sand layer on the
44 delta top. Delta top syn-kinematic sedimentation was maintained at a
45 constant position relative to delta front. This resulted in a slow incremental
46 advance of the delta top syn-kinematic sedimentation per timestep. Delta toe
47 sedimentation was performed by hand sieving a thin 1-3 mm layer of dry
48
49
50
51
52
53
54
55
56
57
58
59
60
61
62
63
64
65

quartz sand above and between the fold belt synclines that terminated 10 cm ahead of the leading fold-thrust. Models with progradational syn-kinematic sedimentation displayed a rapid outward deformation front advance, and hence Models 3 & 5 were designed with a double-length basal polymer layer to reduce distal polymer layer pinchout boundary effects (Fig. 4).

2.2 Basement steps

The Series 1 models had a featureless, horizontal basement overlain by a 1 cm-thick polymer layer (Fig. 3a & Table 1). The Series 2 models had basement steps that were oriented to simulate the Niger Delta oceanic fracture zones relative to the delta top (Fig. 3 & Table 1). The basement steps were infilled by a flat-topped polymer layer that partitioned the basal polymer thicknesses along-strike (Fig. 3). The thickest basal polymer was located within basement Domains B & C, consistent with regional Niger Delta sediment thickness (Fig. 3c) and 2D seismic profiles that show thickened Akata Formation overpressured shales between the Chain and Charcot fracture zones (Morgan, 2004). The Series 2 basement configuration did not attempt to model other localised oceanic basement ridges and smaller-scale grabens documented by seismic studies (e.g. Davies et al., 2005; Briggs et al., 2009), but their potential effects are later discussed in Section 4.

2.3 Materials and scaling

1 Dry quartz sand has a Navier-Coulomb rheology and has been used
2 extensively to simulate the brittle deformation of sedimentary rocks in the
3
4 upper 10 km of the Earth's crust (e.g. Malavieille, 1984; McClay, 1990). The
5
6 dry quartz sand used in the experiments had a density of 1.42 g/cm^3 and a
7
8 cohesion of 95 to 105 Pa. Ring shear testing of the sand indicated the
9
10 following angles of internal friction: an initial peak angle of 33.8° , a stable
11
12 static angle of 33.5° , and a stable dynamic angle of 31.3° .
13
14
15
16
17
18

19 SGM36 is a trade name for polydimethylsiloxane (PDMS), a Newtonian
20
21 viscous material manufactured by Dow Corning Ltd. It has a density of 965 kg
22
23 m^{-3} and an effective viscosity of 19-24 kPa s at a temperature of 25°C
24
25 (Weijermars, 1986). The use of SGM36 in analogue modelling is well
26
27 documented (cf. Weijermars, 1986). SGM36 has been widely used to
28
29 simulate ductile substrates such as salt or overpressured shales in analogue
30
31 experiments (e.g. Ge et al., 1997; McClay et al., 1998; McClay et al., 2000;
32
33 McClay et al., 2003). Here it is noted that shales are plastic and deform only
34
35 after deviatoric stresses overcome the shale strength (cf. Rowan et al. 2004;
36
37 Morency et al., 2007), whereas the viscous SGM polymer will instantly deform
38
39 after loading. For our experiments, overpressured shale plastic behaviour
40
41 was approximated by instantaneously loading the viscous polymer with the
42
43 initial differential load (i.e. the initial delta lobe in Fig. 2a).
44
45
46
47
48
49
50
51
52

53 The scaling factor between model and prototype was 10^{-5} such that 1 cm in
54
55 the models was approximately 1 km of brittle, sedimentary rock in the upper
56
57 crust (cf. McClay, 1990). The time scaling factor of the experiments was 10^{-9}
58
59
60
61
62
63
64
65

1 to 10^{-10} . This timescale was appropriate to simulate instantaneous loading by
2 very rapid sedimentary progradation (Vendeville et al., 1987).
3
4
5
6

7 *2.4 Basal polymer boundaries*

8
9

10
11 The edge of shale overpressures is a parameter that has potential influence
12 on gravity-driven deformation but is not well-constrained at the Niger Delta.
13
14 Studies of overpressured shales suggest that the distal overpressure
15 boundary will move dynamically outward ahead of the deformation front (e.g.
16 Cobbold et al., 2009; Ings and Beaumont, 2010), which implies that delta toe
17 advance is usually not limited by the edge of overpressure. In the
18 experiments presented here, overpressured shales were simulated by either a
19 single-length (i.e. 80 x 100 cm) or a double-length (158 x 100 cm) static basal
20 polymer layer (Fig. 4). The static basal polymer layer was designed to be
21 long enough to allow forward delta advance with minimal edge effects. In the
22 experiments presented here, overpressured shales were simulated by either a
23 single-length (i.e. 80 x 100 cm) or a double-length (158 x 100 cm) static basal
24 polymer layer (Fig. 4). The static basal polymer layer was designed to be
25 long enough to allow forward delta advance with minimal edge effects.
26 However, the static dimensions of the simplified overpressured shale proxy
27 (i.e. the basal polymer) coupled with delta progradation inevitably produced
28 edge effects. These edge effects are carefully described in the model results
29 and included a linear extensional fault across the proximal polymer edge and
30 a linear fold belt across the distal polymer edge.
31
32
33
34
35
36
37
38
39
40
41
42
43
44
45
46
47
48
49
50

51 *2.5 Monitoring and analysis*

52
53
54
55

56 During the experiments the top model surface was photographed at 1 minute
57 intervals. In Models 2 to 5 a laser scanner also recorded the surface
58
59
60
61
62
63
64
65

1 topography at hourly intervals. At the end of the experiments the completed
2 models were impregnated with a gelling agent, serially sectioned at 4 mm
3 increments and photographed. Photographs from the serial sections were
4 used to reconstruct the internal geometries of the models using Paradigm
5 VoxelGeo seismic interpretation software (e.g. Wu et al., 2009; Frankowicz et
6 al., 2009). Digital image correlation (DIC) and strain analysis of the top
7 surface photographs was conducted using LaVision 2D optical deformation
8 and surface flow monitoring software (cf. Adam et al., 2005).

21 **3. Experimental Results**

26 All analogue model illustrations show the progradation direction of the model
27 deltas from left to right. The left-hand side of the model with the delta top is
28 herein referred to as 'landward' and the right-hand side is 'seaward'. Plan
29 view photographs are shown for Model 1, whereas photographs for
30 subsequent experiments are shown in the supplemental material (Figs. S1 to
31 S6).

43 *3.1 Series 1 Experiments*

48 *Model 1 – Aggradational syn-kinematic sedimentation, featureless basement*

53 At 2 hours of differential loading, the delta top formed arcuate grabens near
54 the shelf-slope break (Figs. 5a & b). Arcuate, segmented folds were formed
55 at the delta toe (Figs. 5a & b). A linear graben formed above the left-hand

basal polymer edge due to its boundary effect (Fig. 5b). DIC analyses show a uniform radial outward spreading pattern and peak spreading velocities at the delta slope (Fig. 6a). Both the delta top extensional strains and delta toe compressional strains displayed an arcuate, linear pattern. A translational zone formed at the delta slope that had little to no strains and high horizontal displacements (Figs. 6d & g).

As Model 1 evolved, new delta top regional and counter-regional faults propagated seaward of older faults that advanced the delta top grabens seaward (Fig. 5d). Dip-oriented, radial grabens initiated at the shelf-slope break (Figs. 5c & d). The radial graben extensional faults propagated up- and down-slope. T-shaped grabens were formed at the shelf-slope break by the near-orthogonal linkage of delta top grabens and radial graben (Figs. 5c & d). At the toe-of-slope a pronounced polymer ridge formed that had minor emergent polymer (Fig. 5f). The delta toe fold belt propagated seaward and had a general forward-breaking sequence (Figs. 5c & d). A fold belt initiated at the right-hand polymer pinchout due to its boundary effect and broke backwards (i.e. from the pinchout back towards the delta toe) (Fig. 5d). DIC analyses showed a continued radial outward spreading pattern (Figs. 6b & c). The slope translational zone became more diffuse and was cut by the radial extensional grabens (Figs. 6f & i). The delta toe compressional strains were arcuate but segmented along-strike (Figs. 6e & f).

Figure 7 shows the final delta morphology and interpreted fault systems. The main extensional systems included: (1) an arcuate delta top grabens sub-

1 parallel to the shelf-slope break, and (2) spoke-like radial grabens at the delta
2 slope p (Fig. 7a). The delta toe formed an arcuate fold belt that showed clear
3 along-strike segmentation (Fig. 7a).
4
5
6
7
8

9
10 In cross-section, the Model 1 delta top was formed by regional and counter-
11 regional growth fault arrays that separated partially grounded rafts (Figs. 7b-f).
12 Growth fault footwalls had reactive polymer 'roller' geometries (Figs. 7b-f). An
13 expulsion rollover formed at the toe-of-slope, seaward of the initial pre-
14 kinematic instantaneous load, and was recorded by a polymer bulge and
15 thickened syn-kinematic layers (Figs. 7b-f). The boundary effect growth fault
16 formed across the left-hand polymer limit was regional-dipping and long-lived
17 (Figs. 7b-f). The delta toe fold belt consisted of tight, isoclinal to overturned,
18 polymer-cored detachment folds (Figs. 7b-f).
19
20
21
22
23
24
25
26
27
28
29
30
31

32
33 The 3D reconstruction of Model 1 permitted visualisation of the final basal
34 polymer geometries, final model top surface, and interpreted fault
35 architectures (Fig. 8). In particular, the final basal ductile polymer layer
36 geometries show the arcuate and segmented nature of the delta top
37 extensional and delta toe contractional structures (Fig. 8a).
38
39
40
41
42
43
44
45
46
47

48 *Models 2 & 3 – Progradational syn-kinematic sedimentation, featureless* 49 *basement* 50 51

52
53
54
55 Models 2 & 3 had progradational syn-kinematic sedimentation (ie. on both the
56 delta top and delta toe) and differed only by their basal polymer layer
57
58
59
60
61
62
63
64
65

1 dimensions (Table 1 & Figure 4). During the experiments, rapid delta toe
2 advance was eventually buttressed by the distal polymer boundary (i.e. edge
3 of overpressure) (e.g. Fig. 9). Here Model 3 is presented in detail because it
4 had a double-length polymer layer that allowed further delta toe advance.
5
6 The full results of Model 2 are shown in the supplemental material (Figs. S1 to
7 S3) and are summarised relative to Model 3 later in this section.
8
9

10
11
12 Model 3 initially formed arcuate plan view delta top grabens and delta toe
13 folds similar to Model 1 (Fig. 9a). The delta load spread radially outward and
14 formed a narrow delta slope translational zone similar to Model 1 (Figs. 9d &
15 j).

16
17
18 As Model 3 evolved, the delta top counter-regional growth faults became
19 dominant, showing higher displacements relative to the regional growth faults
20 (Figs. 9b & c). The delta slope and inner delta toe were cut by oblique
21 extensional tear faults (Figs. 9c & i). The tear faults formed within the
22 translational zone and accommodated differential radial spreading (Figs. 4k &
23 l). The delta toe fold belt advanced rapidly and had very active, segmented
24 frontal folds (Figs. 9c & i). A second boundary effect fold belt formed above
25 the right-hand polymer that had closely-spaced, linear folds (Fig. 9c). DIC
26 analyses showed a general radial spreading pattern and rapid broadening of
27 the translational zone (Fig. 9). Model 2 had a similar initial evolution to Model
28 3 but was clearly buttressed by the distal polymer pinchout after 8 hours of
29 deformation (Figs. S1 to S3). The Model 2 delta toe fold belt formed a high
30
31
32
33
34
35
36
37
38
39
40
41
42
43
44
45
46
47
48
49
50
51
52
53
54
55
56
57
58
59
60
61
62
63
64
65

relief fold across the distal polymer edge and an extensive delta toe tear fault array (Figs. S1 to S3).

The final Model 3 delta top had similarities to Model 1 but had dominant counter-regional growth faults (Figs. 10a, b to f). The Model 3 delta toe fold belt was formed by buried and widely-spaced, forward-vergent folds above a broad swell of inflated polymer (Figs. 10b to f).

3.2 Series 2 Experiments

Model 4 – Aggradational syn-kinematic sedimentation and basement steps

Model 4 had the same initial parameters as Model 1 but was underlain by basement steps (Table 1 & Fig. 3). During the experiment, the delta top aggradational syn-kinematic sedimentation also included parts of the delta slope to maintain the prescribed lobate syn-kinematic sedimentation pattern.

At the initial stages arcuate delta top grabens and delta toe folds formed that were segmented across the basement steps (Fig. 11a). The delta toe fold belt formed a slight salient across Domains B & C, which were underlain by thicker basal polymer (Figs. 11a & g). Similar to other models a boundary effect linear graben initiated above the inboard basement step (Fig. 11a). DIC analyses showed subradial outward spreading at Domain A (Fig. 11d). In contrast at Domains B & C had higher spreading velocities and spreading directions were aligned sub-parallel to the basement steps (Fig. 11d).

1
2 As Model 4 evolved, the delta top grabens advanced by initiating new delta
3
4 top extensional faults seaward of older faults similar to Model 1 (Figs. 11b &
5
6 c). Extensional grabens initiated at the delta slope above older, buried delta
7
8 toe fold-thrusts (e.g. Figs. 11b & c). These slope grabens were conspicuous
9
10 by their narrow widths and had similar spacings to the delta toe folds (e.g.
11
12 Figs. 11b & c). The sub-arcuate delta toe fold belt continued to advance
13
14 seaward (Fig. 11b). A second fold belt that had linear folds initiated at the
15
16 right-hand polymer pinchout due to its boundary effect (Fig. 11b). Oblique
17
18 extensional tear faults formed across the basement steps (Figs. 11b & k).
19
20 The tear faults showed extensional strains and accommodated divergent
21
22 spreading across the basement steps (e.g. Fig. 11e). Peak horizontal
23
24 displacements were centred at Domain B and seaward of the inboard
25
26 basement step (Fig. 11k).
27
28
29
30
31
32
33
34
35

36 The final laser scan and 3D basal polymer reconstruction revealed subarcuate
37
38 delta top grabens and delta toe folds (Figs. 12a & 13). These structures were
39
40 segmented across the basement steps by oblique extensional tear faults that
41
42 were cored by a polymer ridge (Figs. 12a & 13). In cross-section, the delta
43
44 top was deformed by regional and counter-regional growth faults and the delta
45
46 toe formed polymer-cored detachment fold trains similar to Model 1 (Figs. 12b
47
48 to e). Growth fault patterns were perturbed near the inboard basement step
49
50 (Fig. 12a). Here expulsion of the thicker initial basal polymer produced a
51
52 large rollover and outboard polymer bulge (Fig. 12d).
53
54
55
56
57
58
59
60
61
62
63
64
65

*Model 5 – Progradational syn-kinematic sedimentation and basement steps,
and double-length polymer layer*

Model 5 initially formed segmented delta top grabens and a subarcuate delta toe fold belt similar to Model 4 (Fig. 14a). A tear fault formed across the Domain B & C basement step (Fig. 14a). Spreading directions were clearly partitioned across the Domain A & B basement step (Fig. 14d). Peak spreading velocities occurred at the delta top and slope across the Domain B & C basement steps (Figs. 14d & j).

As Model 5 evolved the delta top grabens stepped forward and counter-regional faults became dominant (Figs. 14b & c). This showed some similarities to Model 3, which also had progradational syn-kinematic sedimentation (Fig. 9). The tear faults formed across the basement steps propagated seaward (Figs. 14b & c). The delta toe fold belt advanced rapidly and was segmented across the basement steps (Figs. 14b & c). DIC analyses show continued dual, divergent outward spreading directions that were partitioned across the central basement step (Figs. 14e & f).

The Model 5 final deformed state had subarcuate delta top grabens and delta toe folds that were highly segmented (Fig. 15a). Oblique extensional tear faults were formed across the basement steps (Fig. 15a). Delta top and slope fault patterns were perturbed near the inboard basement step (Fig. 15a). The final Model 5 cross-section geometries showed similarities to Model 3, including dominant counter-regional growth faults relative to the regional

1 growth faults and buried, low-amplitude forward and backward-vergent delta
2 toe fold-thrusts above a broad polymer swell (e.g. Figs. 15b to f). Near the
3
4 inboard basement step, expulsion of the thicker initial basal polymer produced
5
6 a large expulsion rollover and outboard polymer bulge (Fig. 15e).
7
8
9

10 11 12 **4. Application to the Niger Delta** 13

14 15 16 *4.1 Evidence for radial spreading* 17

18
19
20
21 Representation deformation styles from the four main models in this study are
22 compared in Figure 16. As first shown by previous studies (e.g. Cobbold and
23
24 Szatmari, 1991; Gaullier and Vendeville, 2005; Loncke et al., 2010; Sellier et
25
26 al., 2013) radial outward spreading in our models produced first-order
27
28 concentric and radial strains (Fig. 16). In our models these strain patterns
29
30 formed regardless of syn-kinematic sedimentation patterns or basement
31
32 configurations (Fig. 16). Similar to previous studies, concentric strains in our
33
34 models were characterised by an arcuate delta top grabens and an arcuate
35
36 delta toe fold belt (e.g. Fig. 16e). Radial strains included segmented delta top
37
38 graben, delta slope radial grabens, delta toe tear faults and segmented delta
39
40 toe fold-thrusts (e.g. Fig. 16e). As first shown by Cobbold and Szatmari
41
42 (1991) and Gaullier and Vendeville (2005), radial and concentric strains are
43
44 characteristic of radial spreading. They are geometric features necessitated
45
46 by the progressive increase in delta lobe radius and lobe perimeter length
47
48 during radial outward spreading.
49
50
51
52
53
54
55
56
57
58
59
60
61
62
63
64
65

1 When compared to the Niger Delta, similarities in radial and concentric strain
2 zonations relative to delta morphology between the models and natural
3
4 prototype provide new evidence for radial spreading at the Niger Delta. In
5
6 particular, both model and prototype have formed segmented counter-regional
7
8 growth faults at the shelf break, delta slope radial grabens, delta toe tear
9
10 faults, and segmented delta toe fold-thrusts (e.g. Figs. 1c & Fig 16). Our
11
12 Model 1 produced distinct plan view T-shaped grabens at the shelf-slope
13
14 break from the linkage of delta top grabens to radial grabens (Fig. 7a). These
15
16 structures are consistent with previous analogue models (e.g. Gaullier and
17
18 Vendeville, 2005) and are highly reminiscent of T-shaped grabens at the
19
20 Niger Delta shelf-slope break (e.g. Rouby et al., 2011).
21
22
23
24
25
26
27
28

29 One difference between our models and the Niger Delta prototype is that the
30
31 basement underlying the inboard Niger Delta has a slight 1° to 3° seaward tilt
32
33 (Fig. 1d). Our Series 1 models had a simplified horizontal basement and did
34
35 not attempt to simulate this feature of the natural prototype. However,
36
37 published analogue models show that a seaward basement tilt has the
38
39 potential to produce more down-to-the-basin (i.e. regional) growth faulting and
40
41 gravity gliding (e.g. Mourgues et al., 2009). These factors may explain why
42
43 the inner Niger Delta top is primarily deformed by regional growth faults (Fig.
44
45 1c) whereas our models formed grabens of paired regional and counter-
46
47 regional growth faults (e.g. Fig. 7). Based numerical modelling results that
48
49 had dynamic basement that was simulated by an elastic beam response (e.g.
50
51 Ings and Beaumont, 2010), it can be inferred that a slight seaward tilt would
52
53
54
55
56
57
58
59
60
61
62
63
64
65

1 have increased deformation along the maximum gradient direction but would
2 not have completely eliminated radial outward spreading.
3
4
5
6

7 *4.2 Effects of Chain and Charcot fracture zone basement steps* 8 9

10
11 In our Series 2 models, as in earlier published experiments (Loncke et al.,
12 2011; Sellier et al., 2013), two divergent spreading directions developed
13
14 across the basement steps (e.g. Fig. 16). Model 5 in this study produced
15
16 spreading patterns that were comparable to the inferred shortening directions
17
18 at the Niger Delta toe (Fig. 17). This suggests that the Niger basement steps
19
20 may have contributed to the formation of the delta toe lobes, but it is important
21
22 to here consider whether the Niger Delta overpressured shales have acted in
23
24 the same manner as the basal polymer in our Series 2 models. The Model 5
25
26 spreading patterns resulted from faster outward flow of the overburden across
27
28 a thicker basal polymer, a well-known effect seen in many analogue models
29
30 (e.g. Loncke et al., 2010). At the Niger Delta, faster outward flows would
31
32 require a thicker or more highly overpressured shale section to substantially
33
34 weaken the shale detachment. The distribution of overpressures at the Niger
35
36 Delta toe is not well-constrained due to a paucity of deepwater well
37
38 penetrations, but it has been generally observed that Niger Delta
39
40 overpressures and fluid flows initiate when the Akata Fm. has reached a
41
42 burial depth of 4 km (Krueger and Grant, 2011). The sedimentary infill is
43
44 generally thicker across the Charcot and Chain fracture zones (e.g. Figs. 1b &
45
46 3c), which allows the possibility for higher overpressures across the Niger
47
48 Delta basement steps.
49
50
51
52
53
54
55
56
57
58
59
60
61
62
63
64
65

1
2 At the Niger Delta top, the growth faults updip of the basement fracture zones
3
4 show uncharacteristic proximal counter-regional growth fault and distal
5
6 regional growth fault patterns (Fig. 17d). Downdip of the basement steps,
7
8 many western lobe toe thrusts have been recently active in contrast to the
9
10 less active southern lobe toe thrusts (Krueger and Grant, 2011). These
11
12 features are potentially explained by the basement step Models 4 & 5 from
13
14 this study, which also developed perturbed inboard delta top growth fault
15
16 patterns and very high delta toe spreading rates across the basement steps
17
18 (Figs. 16c & d, g & h). Although some of the perturbed delta top fault patterns
19
20 in our models could be explained by the inboard basement step geometry
21
22 (Fig. 3), similar perturbed delta top fault patterns have also formed in other
23
24 analogue models without an inboard step (e.g. Loncke et al., 2011).
25
26
27
28
29
30
31
32
33

34 One notable difference between model and natural prototype is that Model 5
35
36 did not form a prominent fold belt re-entrant similar to the Niger Delta toe (Fig.
37
38 14a), despite the apparent similarity in spreading directions (Fig. 17). This
39
40 may indicate that the Niger Delta toe re-entrant geometry is controlled in part
41
42 by buttressing along a Charcot Fracture Zone basement high similar to Briggs
43
44 et al. (2009), a localised feature that we did not attempt to simulate in the
45
46 models presented here. The Niger Delta toe re-entrant directly overlies the
47
48 Charcot Fracture Zone, and correlations between the two features have also
49
50 been implied by many earlier studies (e.g. Corredor et al., 2005; Cobbold et
51
52 al., 2009).
53
54
55
56
57
58
59
60
61
62
63
64
65

4.3 Limitations of the analogue models

As previously mentioned, the range of structural styles formed at the model delta toes presented here were limited by the analogue modelling materials. Our models formed symmetric to asymmetric polymer-cored detachment fold styles that did not resemble the Niger Delta toe imbricate thrust arrays (e.g. Figs. 1d & 7). The detachment fold styles in our models are typical above salt or relatively weak shale décollements whereas the Niger Delta imbricate thrust arrays are more typical of a strong, frictional detachment (Rowan et al., 2004). These differences between model and natural prototype suggest that the overpressured shale detachments below the Niger Delta are stronger (i.e. more frictional) than the sand-polymer proxy in this study. In Models 3 & 5, delta toe syn-kinematic sedimentation strengthened the overburden and produced forward and backward-vergent contractional structures that had more similarities to imbricate thrusts (e.g. Fig.10). Imbricate thrust arrays have also been produced by analogue models that used only frictional Coulomb materials (i.e. dry sand) and compressed air (e.g. Cobbold and Castro, 1999; Mourgues et al., 2009; Cobbold et al., 2009). Nonetheless, at the first-order, regional-scale similarities between our models and Niger Delta prototype suggest that similar strain patterns will form by radial outward gravity spreading above either a weak or a strong shale detachment.

In our models, the plastic behaviour of overpressured shales was approximated by instantaneously loading the viscous polymer with a lobate differential load (i.e. the delta top). This simplified the initial stages of Niger

1 delta progradation and did not permit progradation from a point source (i.e.
2 fluvial system). As a consequence, our model delta top extensional strains
3
4 were localised behind the shelf-slope break (Fig. 5). Our model delta top
5
6 extensional strains appear similarly located relative to Niger Delta top
7
8 extensional strains, which have been primarily coupled to the delta front since
9
10 the Plio-Pleistocene (Rouby et al., 2011). Hence, greater delta top
11
12 progradation of our model deltas would have formed more forward-stepping
13
14 growth fault belts more similar to the Niger Delta prototype.
15
16
17
18
19
20

21 Our experiments used only dry sand to simulate the Niger Delta overburden.
22
23 However, the proximal Niger Delta is subaerial whereas the distal toe is in a
24
25 subaqueous setting. Whereas analogue modelling techniques for submerged
26
27 systems are currently in development, numerical models have compared
28
29 gravity-driven delta deformation in subaerial and subaqueous settings
30
31 (Gemmer et al., 2005). The water column acted as a horizontal buttress force
32
33 that stabilised the overburden and reduced deformation, and the saturated
34
35 sediments reduced differential pressures between overburden and substrate
36
37 (Gemmer et al., 2005). These factors affected local structures but had
38
39 relatively similar outcomes at larger regional scales (Gemmer et al., 2005).
40
41
42
43
44
45
46
47

48 *4.4 Implications for hydrocarbon exploration*

49
50
51
52

53 Our modelling results suggest that faster spreading has occurred across the
54
55 Chain and Charcot fracture zone basement steps relative to the rest of the
56
57 offshore Niger Delta. At a broad regional scale, this would imply higher trap
58
59
60
61
62
63
64
65

1 risks at the Niger Delta western lobe relative to the southern lobe due to
2 reactivated structures. Our results also highlight trap risks at very active tear
3 faults and thrust transfer zone-type structures formed across Chain and
4 Charcot fracture zone basement steps. On the other hand, it has already
5 been shown by Morgan (2003) that the delta toe tear fault systems are
6 conduits for deepwater channel systems and play an important role for
7 reservoir sand distributions. Finally, our models results explain that T-shaped
8 grabens near the Niger Delta shelf-slope break have formed due to radial
9 spreading (e.g. Fig. 5d). Based on our results, these T-shaped grabens form
10 by progressive linkage of shelf-break extensional faults with delta slope radial
11 graben and could be a previously unrecognised shelf or slope play.
12
13
14
15
16
17
18
19
20
21
22
23
24
25
26
27
28

29 **5. Conclusions**

30
31
32
33
34 Comparison of the analogue model results from this study to the Niger Delta
35 have provided the following insights on Niger Delta gravity-driven deformation:
36
37

- 38 (1) Outward radial gravity spreading of the lobate Niger Delta top is
39 evidenced by dip-oriented, extensional structures that include delta
40 slope radial grabens and oblique extensional delta toe tear faults.
41
42 Radial spreading has likely increased the segmentation of Niger delta
43 top growth faults and delta toe fold-thrusts.
44
45
- 46 (2) The analogue models presented here indicate the potential for
47 partitioned gravity spreading across the Chain and Charcot fracture
48 zones basement steps due to changes in the overpressured Akata Fm.
49 shale detachment. The models show that faster gravity spreading
50
51
52
53
54
55
56
57
58
59
60
61
62
63
64
65

north of the Charcot fracture zone could produce dual, divergent spreading directions at the Niger Delta toe that could have contributed to the formation of the Niger Delta toe dual lobes. Other effects include perturbed updip growth fault systems and localised delta toe tear faults. The spreading patterns shown in the models presented here imply that the Niger Delta western lobe toe thrusts have been very active relative to the southern lobe. This would have implications for trap risks for hydrocarbon exploration at the Niger Delta toe.

Acknowledgements

The Shell 4D Deepwater Fold Belts research project provided funding for Jonny Wu's Ph.D. research. Edyta Frankowicz's postdoctoral research was funded by the STAR research project supported by BP, BG Group, BHP Billiton, ConocoPhillips, Nexen, ONGC, PDVSA, RepsolYPF, Shell, Statoil and Talisman. We wish to thank Mike Craker for assistance with the modelling apparatus. Kevin D'Souza is thanked for his valuable photography expertise and management of the analogue modelling lab. Frank Lehane provided timely computer expertise. Juergen Adam is thanked for training on Digital Image Correlation (DIC) analysis and the ring shear tester. We benefited from discussions with Amelie Leduc, Frank Love and Mike Malhaffie. Paradigm Geophysical is thanked for providing VoxelGeo and 3D Canvas seismic interpretation software to the Fault Dynamics Research Group. Lars Backstrom, Umar Ngala, Diego Costantino, Rob Barnes, Frank Despinois, Nicola Scarselli and Nancy Schmidt generously assisted with the experiments. Jose De Vera is thanked for helpful discussions on model reconstruction fault interpretations. The manuscript was considerably improved by the thorough and constructive feedback of two anonymous reviewers.

References

- Adam, J., Urai, J. L., Wieneke, B., Oncken, O., Pfeiffer, K., Kukowski, N., Lohrmann, J., Hoth, S., van der Zee, W. and Schmatz, J., 2005. Shear localisation and strain distribution during tectonic faulting - new insights from granular-flow experiments and high-resolution optical image correlation techniques. *Journal of Structural Geology*, 27, 2, 283–301.
- Alzaga-Ruiz, H., Granjeon, D., Lopez, M., Seranne, M. and Roure, F., 2009. Gravitational collapse and Neogene sediment transfer across the western margin of the Gulf of Mexico: Insights from numerical models. *Tectonophysics*, 470, 1-2, 21–41.
- Briggs, S. E., Davies, R. J., Cartwright, J. and Morgan, R., 2009. Thrusting in oceanic crust during continental drift offshore Niger Delta, equatorial Africa. *Tectonics*, 28, 1, TC1004.
- Cobbold, P. R. and Szatmari, P., 1991. Radial gravitational gliding on passive margins. *Tectonophysics*, 188, 3-4, 249–289.
- Cobbold, P. R., Clarke, B. J. and Loseth, H., 2009. Structural consequences of fluid overpressure and seepage forces in the outer thrust belt of the Niger Delta. *Petroleum Geoscience*, 15, 1, 3–15.
- Corredor, F., Shaw, J. H. and Bilotti, F., 2005. Structural styles in the deep-water fold and thrust belts of the Niger Delta. *AAPG Bulletin*, 89, 6, 753–780.
- Davies, R.J., MacLeod, C.J., Morgan, R., Briggs, S.E., 2005. Termination of a fossil continent-ocean fracture zone imaged with three-dimensional seismic data: The Chain Fracture Zone, eastern equatorial Atlantic. *Geology*, 33, 8, 641-644.
- Doust, H. and Omatsola, E., 1990. Niger Delta, in: Edwards, J. D. and Santogrossi, P. A., (Eds.), *Divergent/Passive Margin Basins*, AAPG Memoir 48. pp. 201–238.
- Evamy, B. D., Haremboure, J., Kamerling, P., Knaap, W. A., Molloy, F. A. and Rowlands, P. H., 1978. Hydrocarbon habitat of the Tertiary Niger Delta. *AAPG Bulletin*, 62, 1–39.
- Frankowicz, E., Wu, J. E., de Vera, J., Ngala, U. McClay, K. 2008. 3D volume reconstruction and visualisation of delta models - applications to seismic interpretation. 2008 AAPG Annual Convention conference abstract.
- Gaullier, V. and Vendeville, B. C., 2005. Salt tectonics driven by sediment progradation: Part II - Radial spreading of sedimentary lobes prograding above salt. *AAPG Bulletin*, 89, 8, 1081–1089.

1 Ge, H., Jackson, M. P. A. and Vendeville, B. C., 1997. Kinematics and
2 dynamics of salt tectonics driven by progradation. AAPG Bulletin, 81, 3, 398–
3 423.

4
5 Gemmer, L., Beaumont, C., Ings, S.J., 2005. Dynamic modelling of passive
6 margin salt tectonics: effects of water loading, sediment properties and
7 sedimentation patterns. Basin Research, 17, 383-402.

8
9
10 Haack, R. C., Sundararaman, P., Diedjomahor, J. O., Xiao, H., Gant, N. J.,
11 May, D., Kelsch, K., 2000. Niger Delta petroleum systems, Nigeria, in: Mello,
12 M. R., Katz, B. J., (Eds.), AAPG Memoir 73, Petroleum systems of South
13 Atlantic margins. pp. 213–231.

14
15
16 Ings, S. J. and Beaumont, C., 2010. Continental margin shale tectonics:
17 preliminary results from coupled fluid-mechanical models of large scale delta
18 instability. Journal of the Geological Society of London, 167, 571–582.

19
20
21 Krezsek, C., Adam, J. and Grujic, D., 2007. Mechanics of fault and expulsion
22 rollover systems developed on passive margins detached on salt: insights
23 from analogue modelling and optical strain monitoring, in: Jolley, S. J., Barr,
24 D., Walsh, J. J. and Knipe, R. J., (Eds.), Structurally Complex Reservoirs,
25 Geological Society, London, Special Publications 292. pp. 103–121.

26
27
28 Krueger, S. W., Grant, N. T., 2011. The growth history of toe thrusts of the
29 Niger Delta and the role of pore pressure, in: McClay, K. R., Shaw, J. H.,
30 Suppe, J., (Eds.), AAPG Memoir 94, Thrust fault-related folding. pp. 357-390.

31
32
33 Lehner, P. and de Ruiter, P. A. C., 1977. Structural history of Atlantic margin
34 of Africa. AAPG Bulletin, 61, 7, 961–981.

35
36
37 Loncke, L., Vendeville, B. C., Gaullier, V. and Mascle, J., 2010. Respective
38 contributions of tectonic and gravity-driven processes on the structural pattern
39 in the Eastern Nile deep-sea fan: insights from physical experiments. Basin
40 Research, in press.

41
42
43 Malavieille, J., 1984. Modelisation experimentale des chevauchements
44 imbriquees: Application aux chaines de montagnes. Bulletin de la Societe
45 Geologique de France, 26, 1, 129–138.

46
47
48 McClay, K. R., 1990. Deformation mechanics in analogue models of
49 extensional fault systems, in: Knipe, R. J. and Rutter, E. H., (Eds.),
50 Deformation Mechanisms, Rheology and Tectonics, Geological Society,
51 London, Special Publication 54. pp. 445–453.

52
53
54 McClay, K. R., Dooley, T. and Lewis, G., 1998. Analog modeling of
55 progradational delta systems. Geology, 26, 9, 771–774.

56
57
58 McClay, K. R., Dooley, T. and Zamora, G., 2003. Analogue models of delta
59 systems above ductile substrates, in: van Rensbergen, P., Hillis, R. R.,
60
61
62
63
64
65

1 Maltman, A. J. and Morley, C. K., (Eds.), Subsurface Sediment Mobilization,
2 Geological Society Special Publication 216. pp. 411–428.

3 Morgan, R., 2003. Prospectivity in ultradeep water: the case for petroleum
4 generation and migration within the outer parts of the Niger Delta apron, in:
5 Arthur, T. J., MacGregor, D. S., Cameron, N. R., (Eds.), Geological Society,
6 London, Special Publications 207, Petroleum geology of Africa: New themes
7 and developing technologies. pp. 151–164.
8
9

10 Morgan, R., 2004. Structural controls on the positioning of submarine
11 channels on the lower slopes of the Niger Delta, in: Davies, R. J., Cartwright,
12 J. A., Stewart, S. A., Lappin, M., Underhill, J. R., (Eds.), Geological Society,
13 London, Memoirs 29, 3D seismic technology: application to the exploration of
14 sedimentary basins. pp. 45–51.
15
16

17 Mourgues, R., Lecomte, E., Vendeville, B. and Raillard, S., 2009. An
18 experimental investigation of gravity-driven shale tectonics in progradational
19 delta. Tectonophysics, 474, 3-4, 643–656.
20
21

22 Rouby, D., Nalpas, T., Jermannaud, P., Robin, C., Guillocheau, F. and
23 Raillard, S., 2011. Gravity driven deformation controlled by the migration of
24 the delta front: The Plio-Pleistocene of the Eastern Niger Delta.
25 Tectonophysics, 513, 1-4, 54–67.
26
27

28 Rowan, M. G., Peel, F. J. and Vendeville, B. C., 2004. Gravity-driven fold
29 belts on passive margins, in: McClay, K. R., (Ed.), Thrust Tectonics and
30 Hydrocarbon Systems, AAPG Memoir 82. pp. 157–182.
31
32

33 Sandwell, D. T. and Smith, W. H. F., 2009. Global marine gravity from
34 retracked Geosat and ERS-1 altimetry: Ridge segmentation versus spreading
35 rate. Journal of Geophysical Research, 114, B1, B01411.
36
37

38 Saugy, I. and Eyer, J. A., 2003. Fifty years of exploration in the Niger Delta
39 (West Africa), in: Halbouty, M. T., (Ed.), Giant oil and gas fields of the decade
40 1990-1999, AAPG Memoir 78. pp. 221–226.
41
42

43 Sellier, N.C., Vendeville, B., and Loncke, L., 2013. Post-Messinian evolution
44 of the Florence Rise area (Western Cyprus Arc) Part II: Experimental
45 modeling. Tectonophysics, 591, 143-151.
46
47

48 Sibuet, J.C. and Mascle, J., 1978. Plate Kinematic Implications of Atlantic
49 Equatorial Fracture Zone Trends. Journal of Geophysical Research, Vol. 83,
50 No. B7, 3401-3421.
51
52

53 Vendeville, B. C., 2005. Salt tectonics driven by sediment progradation: Part I
54 - Mechanics and kinematics. AAPG Bulletin, 89, 8, 1071–1079.
55
56

57 Vendeville, B., Cobbold, P. R., Davy, P., Choukroune, P. and Brun, J. P.,
58 1987. Physical models of extensional tectonics at various scales, in: Coward,
59
60
61
62
63
64
65

1 M. P., Dewey, J. F. and Hancock, P. L., (Eds.), Continental Extensional
2 Tectonics, Geological Society, London, Special Publication 28. pp. 95–107.

3
4 Weijermars, R., 1986. Flow behaviour and physical chemistry of bouncing
5 putties and related polymers in view of tectonic laboratory applications.
6 Tectonophysics, 124, 3-4, 325–358.

7
8
9 Wu, J. E., McClay, K., Whitehouse, P. and Dooley, T., 2009. 4D analogue
10 modelling of transtensional pull-apart basins. Marine and Petroleum Geology,
11 26, 8, 1608–1623.
12
13
14
15
16
17
18
19
20
21
22
23
24
25
26
27
28
29
30
31
32
33
34
35
36
37
38
39
40
41
42
43
44
45
46
47
48
49
50
51
52
53
54
55
56
57
58
59
60
61
62
63
64
65

Figure Captions

Figure 1: a) Location map of the Niger Delta and the offshore Chain and Charcot oceanic fracture zones shown by onshore SRTM3 digital elevation model and offshore free-air gravity data (Sandwell and Smith, 2009). Note the delta sediments deposited across the basement fracture zones. FZ = Fracture Zone. b) Lobate shape of the Niger Delta clastic wedge revealed by a total sediment thickness isopach map (redrawn from Cobbold et al., 2009). The landward termination of the fracture zones is not well constrained. c) Niger Delta structural map (modified from Saugy and Eyer, 2003; Krueger and Grant, 2011). d) Schematic 2:1 vertical exaggeration cross-section across the Niger Delta (modified from Haack et al., 2000; Rouby et al., 2011). Cross-section location is shown in c).

Figure 2: 3D schematics showing experimental setup for the gravity-driven delta analogue models. a) Geometry of the pre-kinematic lobate differential load and the ductile polymer substrate. The cutaway reveals the polymer geometry. b) Syn-kinematic sand layers were progressively added to the delta top and/or delta toe during the experiment. Details for specific experiments are shown in Figure 4. c) Analogue model layering shown by photographs and line diagram. Pre-kinematic sand layers were coloured alternating blue, black and white whereas syn-kinematic sand layers were coloured alternating red and white.

Figure 3: Basement configurations for the analogue models in this study in comparison to the Niger Delta prototype. a) Series 1 models had flat, horizontal featureless basement whereas b) Series 2 had basement steps patterned after the Chain and Charcot fracture zones, offshore Niger Delta. c) Niger Delta total sediment thickness isopach map from Fig. 1b, reoriented for comparison to a) & b). d) Schematic 3D view of Series 2 basement steps.

Figure 4: Model for the 3D gravity-driven delta analogue models presented here. Series 1 models had a horizontal basement whereas Series 2 models had basement steps. Syn-kinematic sedimentation patterns were varied between 'aggradational' and 'progradational'. The basal polymer layer was doubled in length in Models 3 & 5 to allow the model deltas to advance further basinward.

Figure 5: Progressive evolution of Model 1 with syn-kinematic sedimentation on the delta top only. Plan view evolution illustrated at a-b) 0.5 hrs, c-d) 7 hrs, e-f) 13.5 hrs using sequential photographs and line drawing interpretations, respectively. Photograph illumination is from the right.

Figure 6: Model 1 evolution analysed using digital image correlation (DIC). a-c) show progressive spreading directions from 2-hour incremental particle movement vectors superimposed on a plan view photograph. d) to f) progressive strain evolution from 2-hour incremental horizontal strain plots. g) to i) show the translational zone from 2-hour incremental total horizontal displacement plots. Model 1 was characterised by uniform radial outward spreading and the formation of arcuate delta top extensional, delta slope

translational, and delta toe compressional zones. Extensional grabens radial to the delta lobe formed at the slope.

Figure 7: a) Final plan view geometries of Model 1 at 13.5 hrs illustrated by the reconstructed final model topography and overlain by structural interpretation. Deformation was characterised by delta top grabens, delta slope radial grabens, an emergent polymer bulge at the delta toe and a delta toe fold belt. b-f) Interpreted internal vertical cross-sections from Model 1. Final slope angles are shown in d). Cross-section locations are shown in a).

Figure 8: 3D visualisation of the Model 1 reconstruction. a) 3D view showing selected cross-sections and the final basal polymer surface. The polymer ridges indicate the delta top graben and radial extensional graben systems. The delta toe fold-thrust belt was arcuate and highly segmented. b) 3D view of the final top surface of the model showing the final lobate delta top differential load. c) Final interpreted fault-fold geometries.

Figure 9: Model 3 with progradational syn-kinematic sedimentation analysed using digital image correlation (DIC) plan view plots at progressive time intervals. a) to c) 2-hour incremental particle displacement vectors overlain on a plan view photograph. d) to f) 2-hour incremental horizontal strains. g) to i) 2-hour incremental horizontal displacements. The translational zone dramatically broadened. The fold belt advanced rapidly, was cut by tear faults, and had very active frontal folds.

Figure 10: a) Final plan view geometries of Model 3 at 11.5 hrs illustrated by laser scan topography overlain by structural interpretation. The delta top grabens had dominant counterregional growth faults and the delta toe was cut by tear faults. b-f) Interpreted internal vertical cross-sections from Model 3. Cross-section locations are shown in a).

Figure 11: Model 4 with aggradational syn-kinematic sedimentation and basement steps analysed using digital image correlation (DIC). a) to c) show interpreted structures from top photographs, d) to f) 2-hour incremental particle displacement vectors overlain on a plan view photograph, g) to i) 2-hour incremental horizontal strains, and j) to l) 2-hour incremental horizontal displacements. Radial outward spreading was partitioned into two principal directions and the structures became segmented across the basement steps.

Figure 12: a) Final plan view geometries of Model 4 at 14.5 hrs illustrated by laser scan topography overlain by structural interpretation. The delta top graben system and delta toe fold belt became segmented above the basement steps. b-e) Interpreted internal vertical cross-sections from Model 4. Final slope angles are shown in c) & d). Cross-section locations are shown in a).

Figure 13: 3D view of the Model 4 reconstruction showing the final basal polymer surface and selected cross-sections. The underlying passive basement steps had differential basal polymer thicknesses of 1, 2 and 1.5 cm thickness in domains A, B & C, respectively. Both delta top and delta toe

structures were segmented across the basement steps. Delta top structures were perturbed up dip of the inboard basement step.

Figure 14: Model 5 evolution analysed using digital image correlation (DIC) plan view plots at progressive time intervals. a) to c) show interpreted structures from photographs, d) to f) 2-hour incremental particle displacement vectors overlain on a plan view photograph, g) to i) 2-hour incremental horizontal strains, and j) to l) 2-hour incremental horizontal displacements. Radial outward spreading was partitioned into two principal directions. The translational zone dramatically broadened and was offset above the basement steps.

Figure 15: a) Final plan view geometries of Model 5 with basement steps and progradational syn-kinematic sedimentation at 12.75 hrs illustrated by laser scan topography and overlain by structural interpretation. Delta top and delta toe structures were segmented across the basement steps. b-e) Interpreted internal vertical cross-sections from Model 5. Cross-section locations are shown in a).

Figure 16: Comparison of plan view digital image correlation (DIC) between Models 1,3,4 & 5 at an intermediate deformation stage. a) to d) 2-hour incremental particle displacement vectors overlain on a plan view photograph. e) to h) 2-hour incremental horizontal strains, i) to l) 2-hour incremental horizontal displacements with main spreading directions indicated by red arrows. All models spread radially outward. Models 3 & 5 with progradational syn-kinematic sedimentation formed a wide translational zone. Models 4 & 5 with basement steps had partitioned spreading directions and segmented strains. All images are at the same scale.

Figure 17: Comparison between analogue models and Niger Delta spreading patterns. a) to c) Model 5 DIC analysis showing 2-hour incremental horizontal translations and spreading directions. d) Niger Delta fault map from Figure 1c, rotated for comparison to the analogue model. The dual, divergent spreading directions developed in Model 5 show similarities to the Niger Delta delta toe shortening directions.

Figure 18: Conceptual model of structures formed by radial spreading across basement steps at the Niger Delta, based on insights from the analogue models in this study.

Table Captions

Table 1: Summary list of analogue experiments of gravity-driven delta systems. Refer to Figure 4 for detailed model configurations.

Supplemental figure captions

Figure S1: Progressive evolution of Model 2 with syn-kinematic sedimentation on both the delta top and delta toe. Plan view evolution illustrated at a-b) 2.75 hrs, c-d) 8 hrs, and e-f) 13.5 hrs using sequential photographs and line

1 drawing interpretations, respectively. Photograph illumination is from the
2 right.

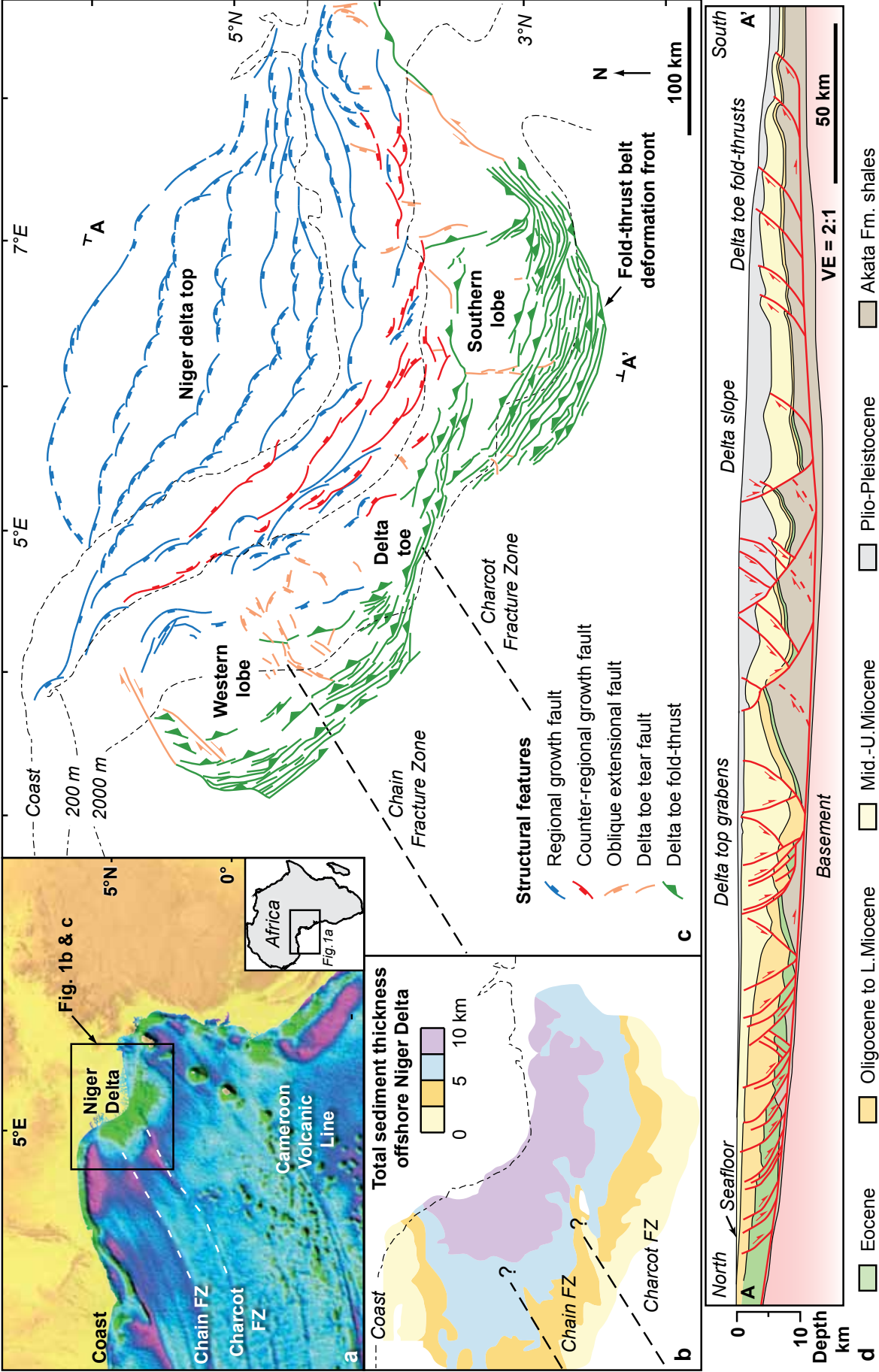
3
4 Figure S2: Model 2 evolution analysed using digital image correlation (DIC) at
5 progressive time intervals. a) to c) 2-hour incremental particle displacement
6 vectors overlain on a plan view photograph. d) to f) 2-hour incremental
7 horizontal strains. g) to i) 2-hour incremental horizontal displacements. The
8 progradational syn-kinematic sedimentation produced dramatic widening of
9 the translational zone and rapid advance of the delta toe fold-thrust belt.
10 Radial outward spreading was buttressed by the distal polymer pinchout and
11 a tear fault array formed at the inner delta toe.
12
13

14 Figure S3: a) Final plan view geometries of Model 2 at 13.5 hrs illustrated by
15 laser scan topography overlain by structural interpretation. b) Interpreted
16 internal vertical cross-section from Model 2. Cross-section location is shown
17 in a).
18
19

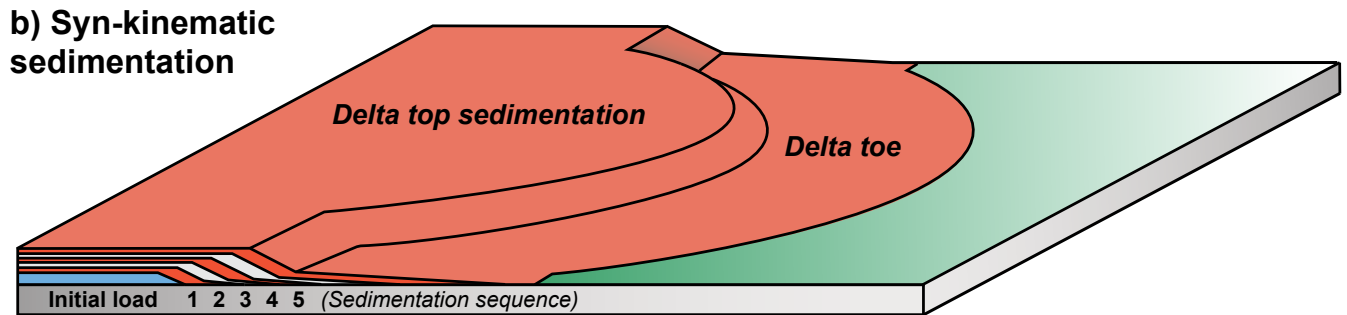
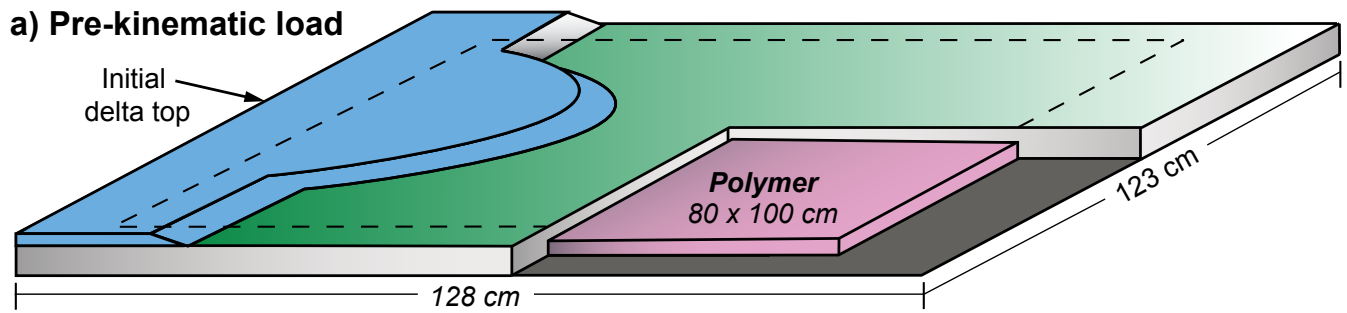
20 Figure S4: Model 3 with syn-kinematic sedimentation on both the delta top
21 and delta toe. The basal polymer layer was doubled in length to allow the
22 delta toe fold belt to propagate further outwards. Plan view evolution
23 illustrated at a-b) 2 hrs, c-d) 8 hrs, and e-f) 11.5 hrs using sequential
24 photographs and line drawing interpretations, respectively. Illumination of the
25 photographs is from the right.
26
27
28

29 Figure S5: Model 4 with syn-kinematic sedimentation on the delta top only.
30 The sandpack was allowed to deform above passive basement steps shown
31 in b). Plan view evolution illustrated at a-b) 2.5 hrs, c-d) 7.25 hrs, e-f) 14.5
32 hrs using sequential photographs and line drawing interpretations,
33 respectively. Photograph illumination is from the right.
34
35

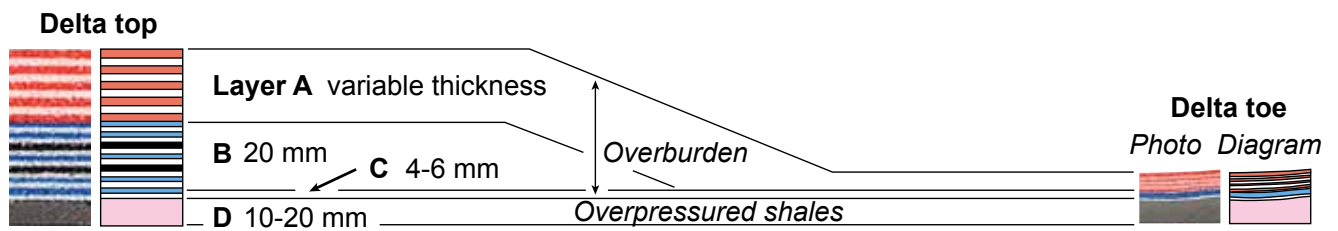
36 Figure S6: Model 5 with syn-kinematic sedimentation on both the delta top
37 and the delta toe. The sandpack was allowed to deform above passive
38 basement steps shown in b). Plan view evolution illustrated at a-b) 2.25 hrs,
39 c-d) 7.5 hrs, and e-f) 12.75 hrs using sequential photographs and line drawing
40 interpretations, respectively. Photograph illumination is from the right.
41
42
43
44
45
46
47
48
49
50
51
52
53
54
55
56
57
58
59
60
61
62
63
64
65



Wu et al. Figure 1



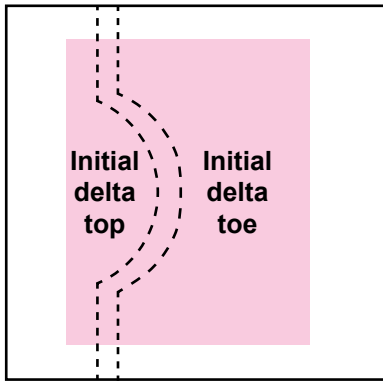
c) Model layering



A = Syn-kinematic; B & C = Pre-kinematic; D = SGM36 polymer

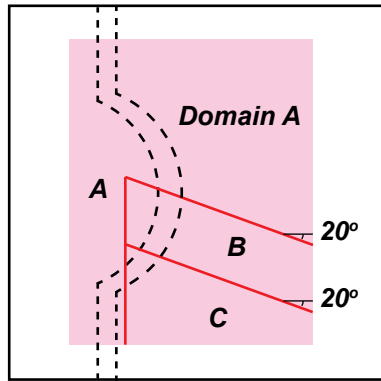
Wu et al. Figure 2

a) Series 1 featureless basement



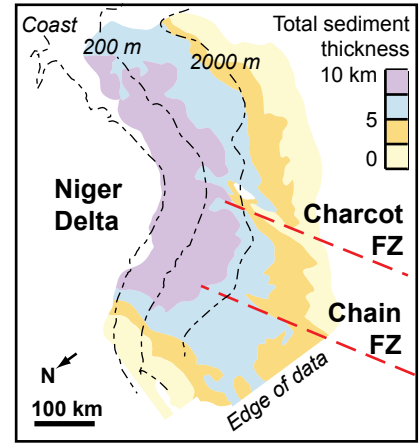
Basal polymer layer
80 x 100 x 1 cm thickness

b) Series 2 basement steps

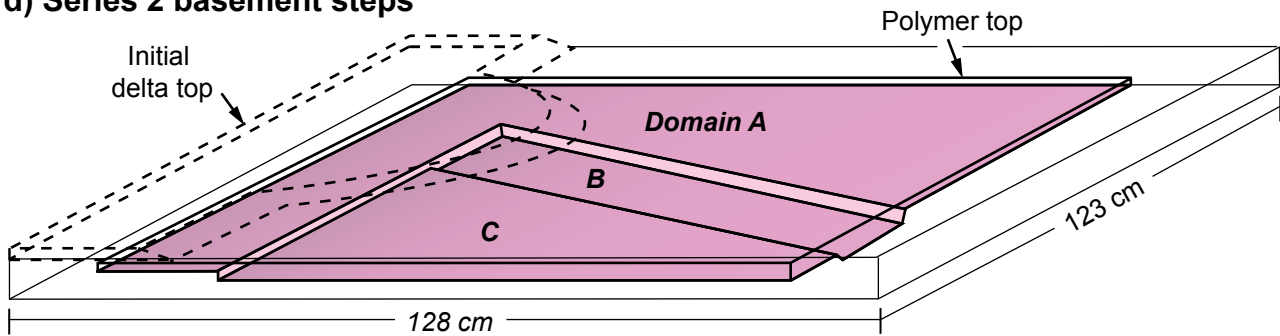


Basement step
Polymer thickness
A - 1 cm; B - 2 cm; C - 1.5 cm

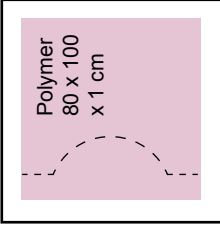
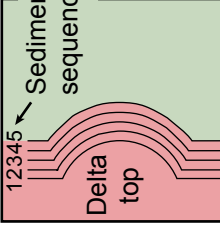

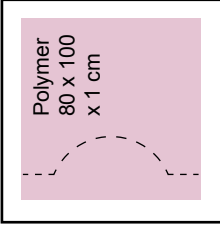
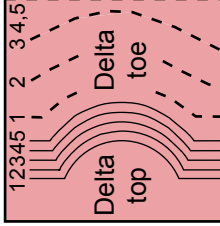

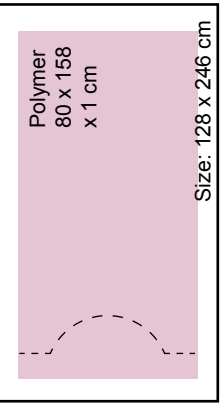
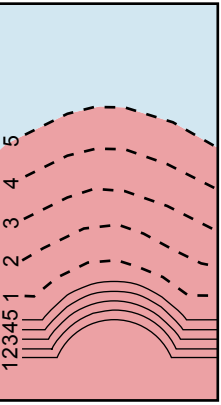

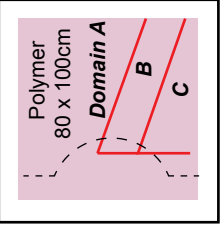
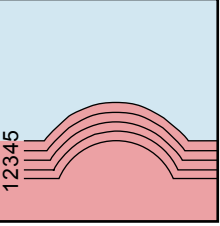

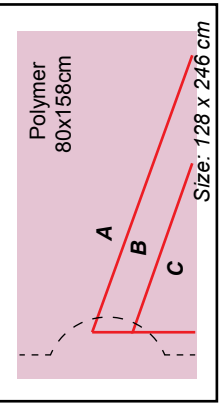
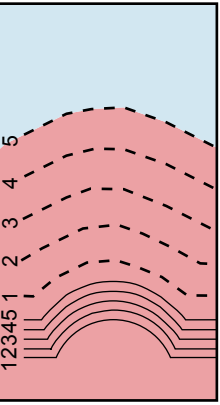

c) Niger Delta setting



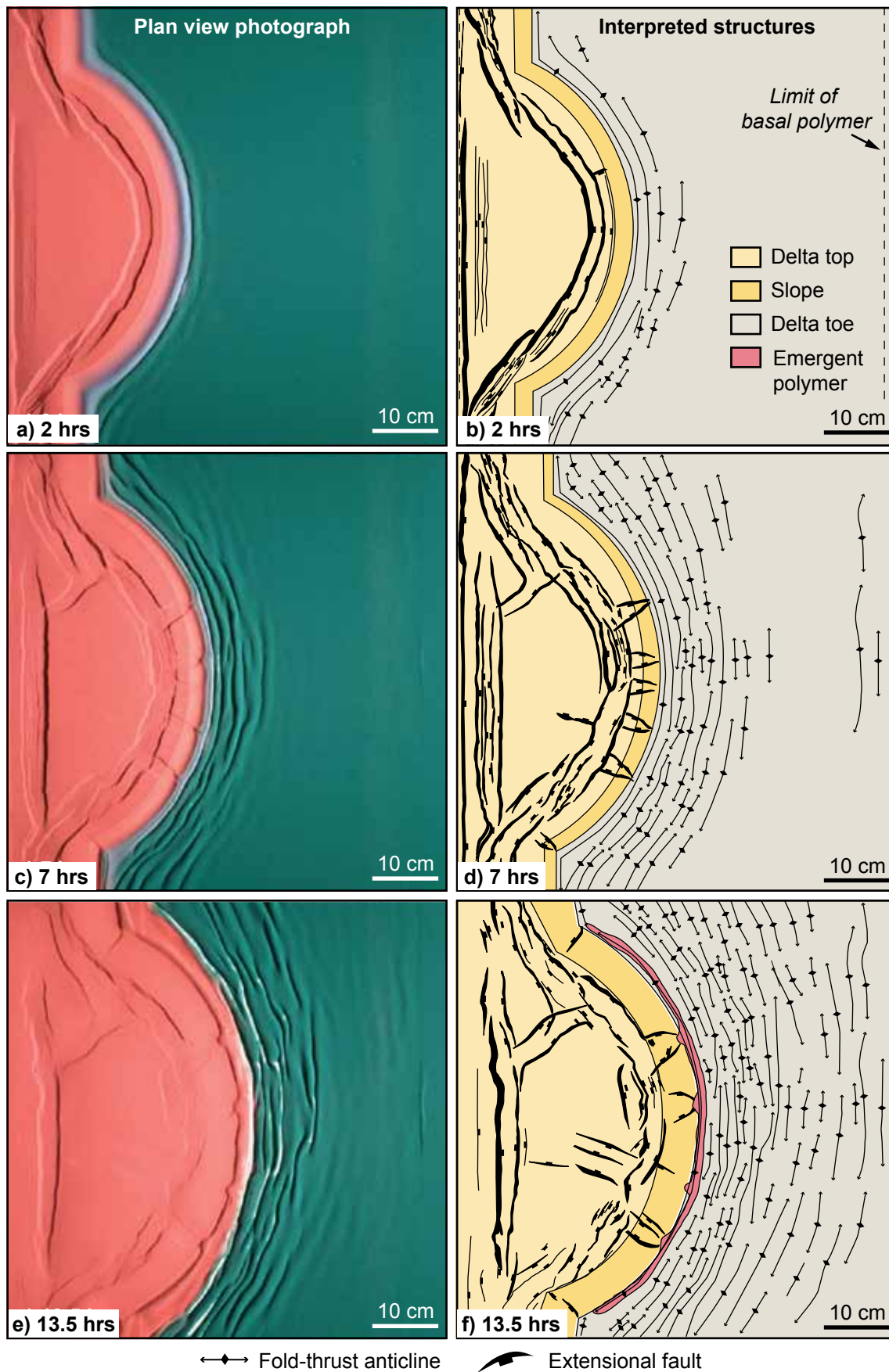
d) Series 2 basement steps



Wu et al. Figure 3

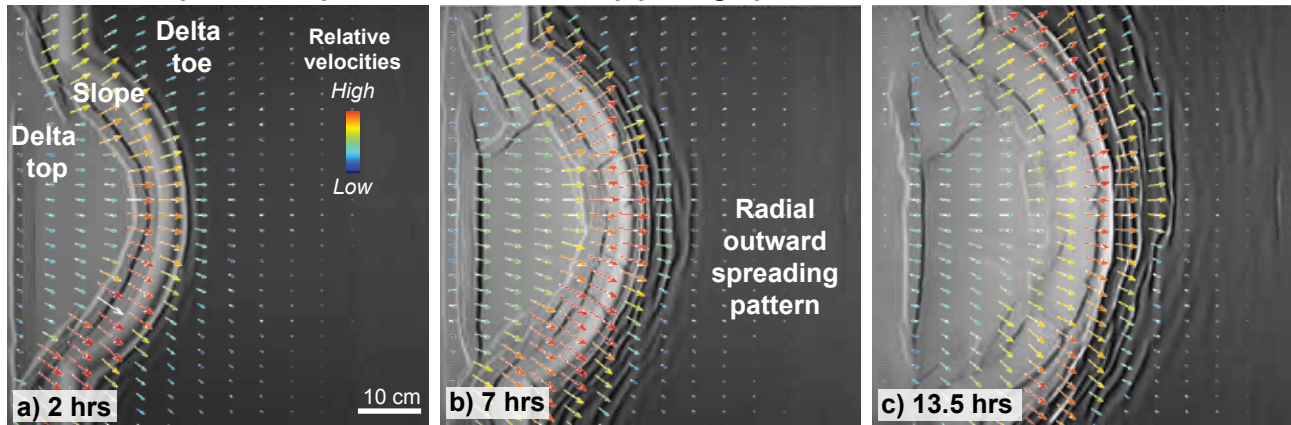
Model number	Model series	Initial model configuration <i>Plan view</i>	Syn-kinematic sedimentation <i>Plan view pattern</i>	Syn-kinematic-sedimentation <i>Cross-sectional view</i>	Time hrs
Model 1 <i>Aggradational sedimentation</i>	1	 <p>Polymer 80 x 100 x 1 cm</p> <p>--- Initial load ■ Polymer</p> <p>Size: 128 x 123 cm</p>	 <p>12345 Sedimentation sequence Delta top Delta toe</p>	 <p>1 2 3 4 5 Sedimentation sequence ■ Syn-kinematic sedimentation ■ Pre-kinematic load</p>	13.5
Model 2 <i>Progradational sedimentation</i>	1	 <p>Polymer 80 x 100 x 1 cm</p> <p>Size: 128 x 123 cm</p>	 <p>12345 Delta top Delta toe</p>	 <p>1 2 3 4 5</p>	13.5
Model 3 <i>Progradational sedimentation</i>	1	 <p>Polymer 80 x 158 x 1 cm</p> <p>Size: 128 x 246 cm</p>	 <p>12345 Delta top Delta toe</p>	 <p>1 2 3 4 5</p>	11.5
Model 4 <i>Aggradational sedimentation & basement steps</i>	2	 <p>Polymer 80 x 100cm Domain A B C</p> <p>Polymer thickness: A - 1 cm B - 2 cm C - 1.5 cm</p> <p>Size: 128 x 123 cm</p> <p>Basement step —</p>	 <p>12345 Delta top Delta toe</p>	 <p>1 2 3 4 5</p>	14.5
Model 5 <i>Progradational sedimentation & basement steps</i>	2	 <p>Polymer 80x158cm</p> <p>Size: 128 x 246 cm</p> <p>A B C</p>	 <p>12345 Delta top Delta toe</p>	 <p>1 2 3 4 5</p>	12.75

Wu et al. Figure 4

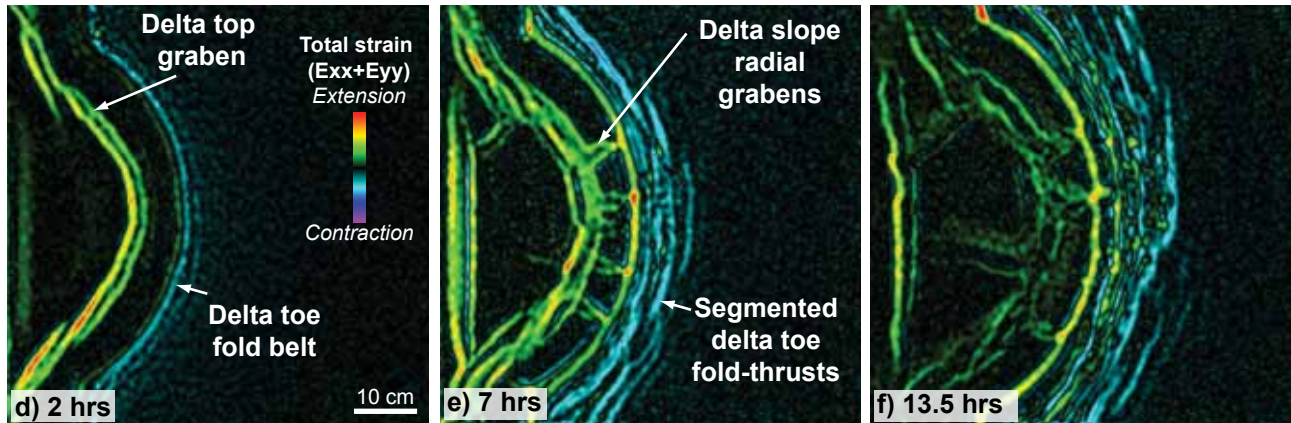


Wu et al. Figure 5

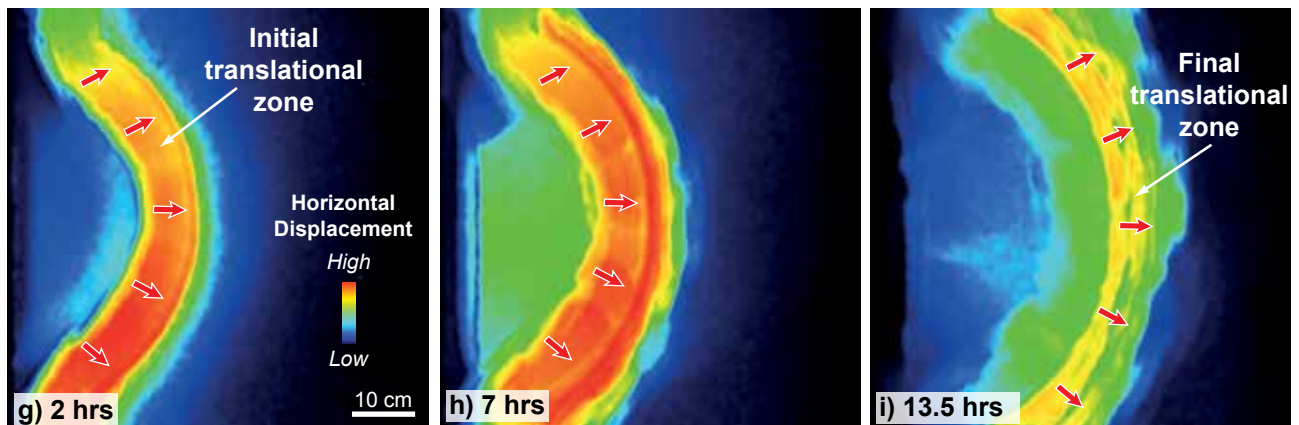
Incremental particle displacement vectors & top photograph



Incremental strain

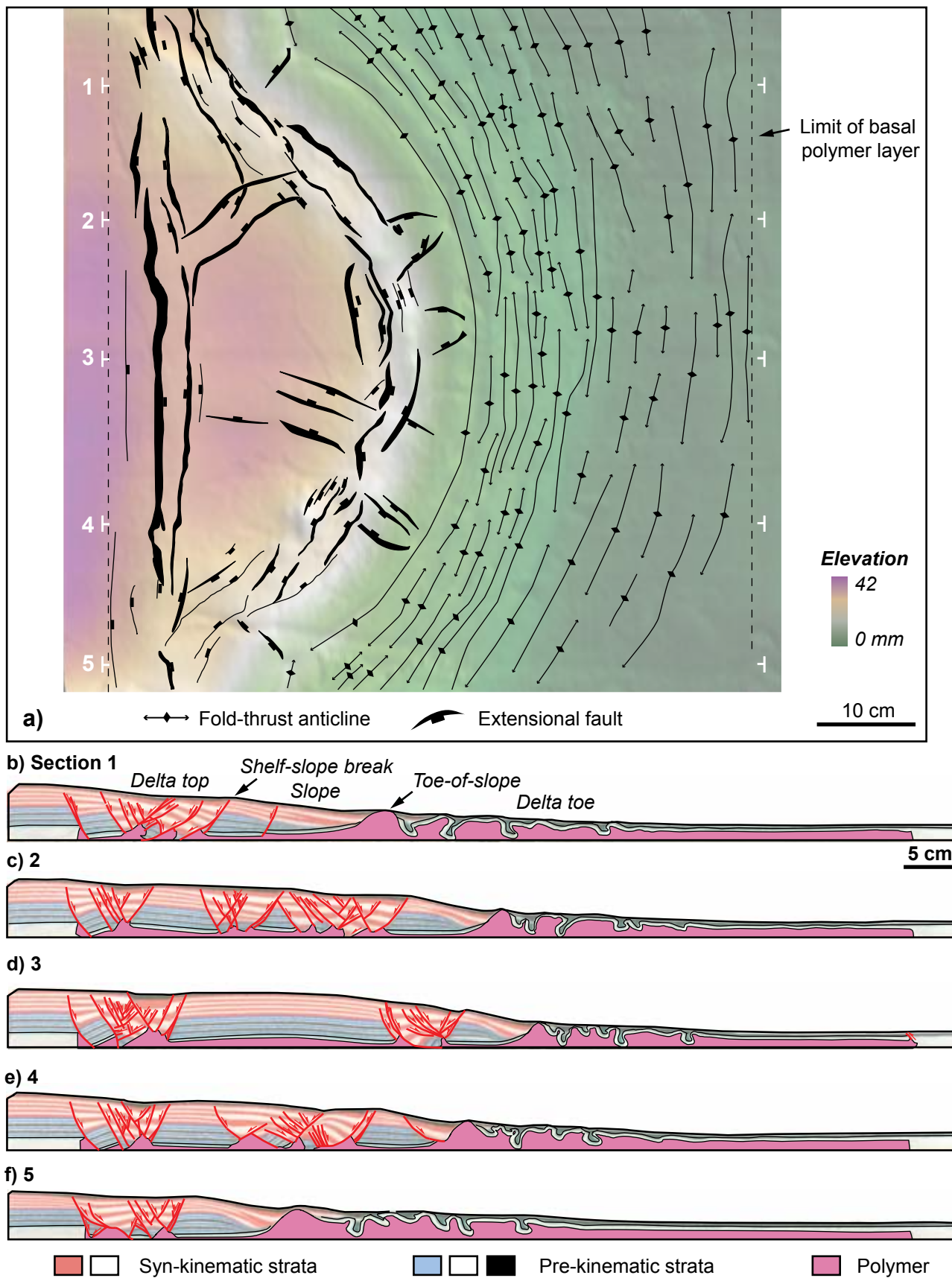


Incremental horizontal displacement

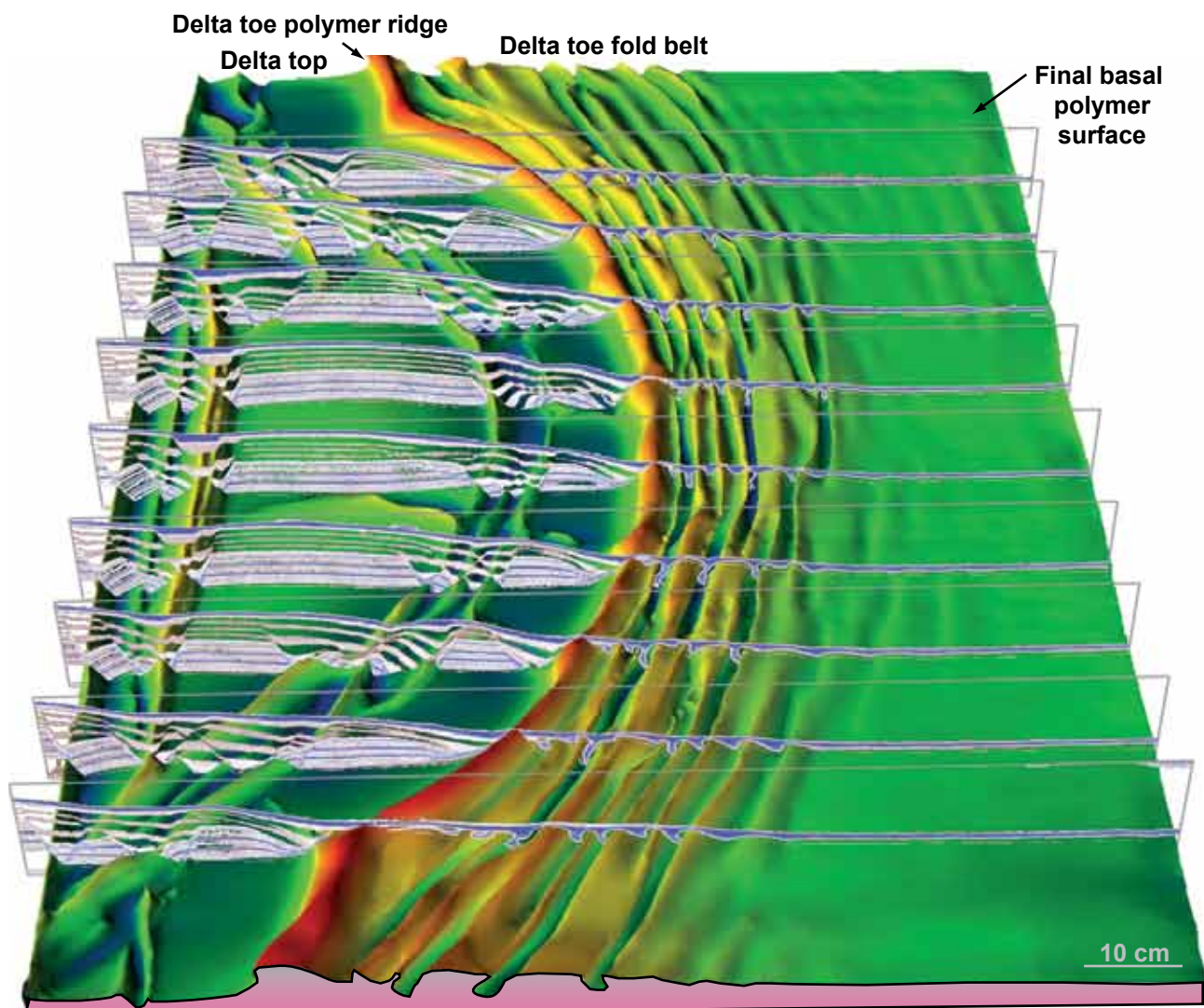


➡ Main gravity spreading directions

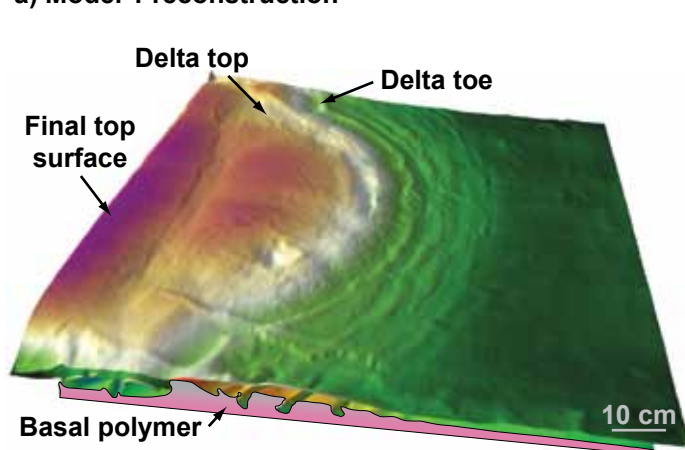
Wu et al. Figure 6



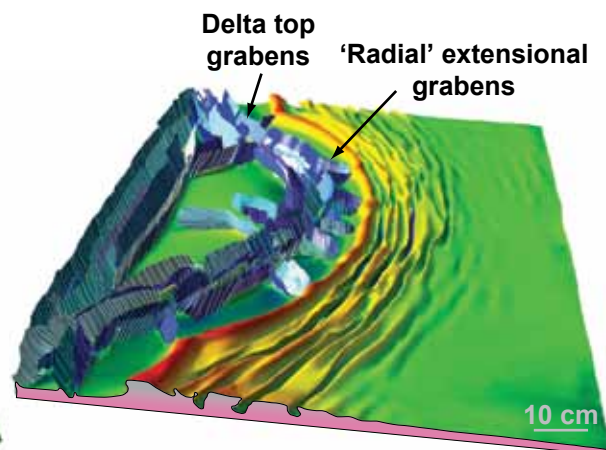
Wu et al. Figure 7



a) Model 1 reconstruction

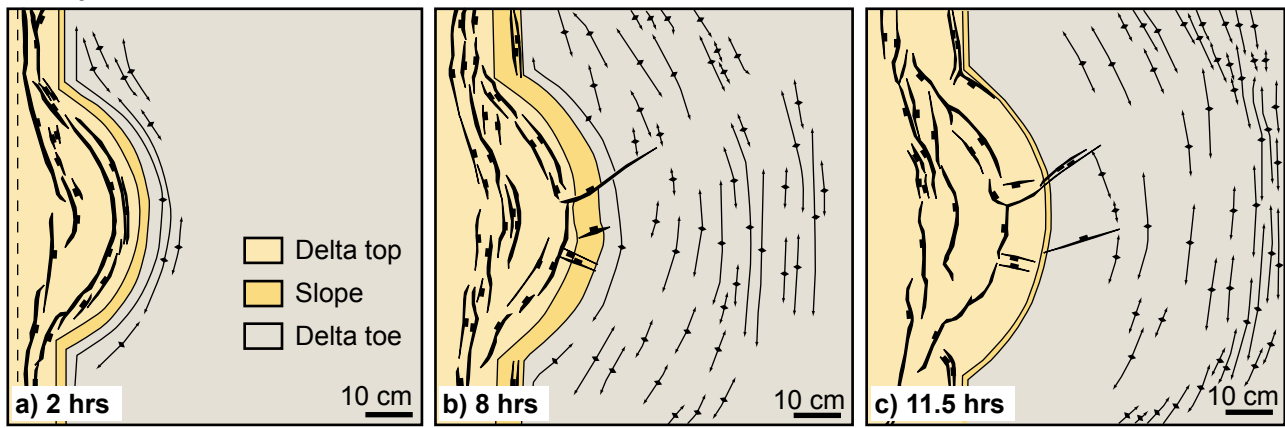


b) Model 1 final top surface

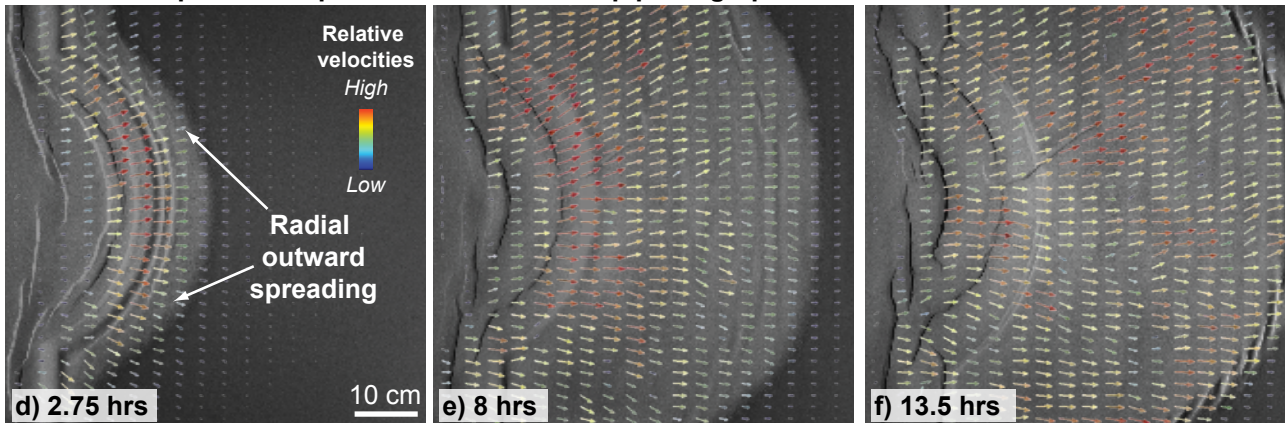


c) Model 1 Interpreted fault geometries

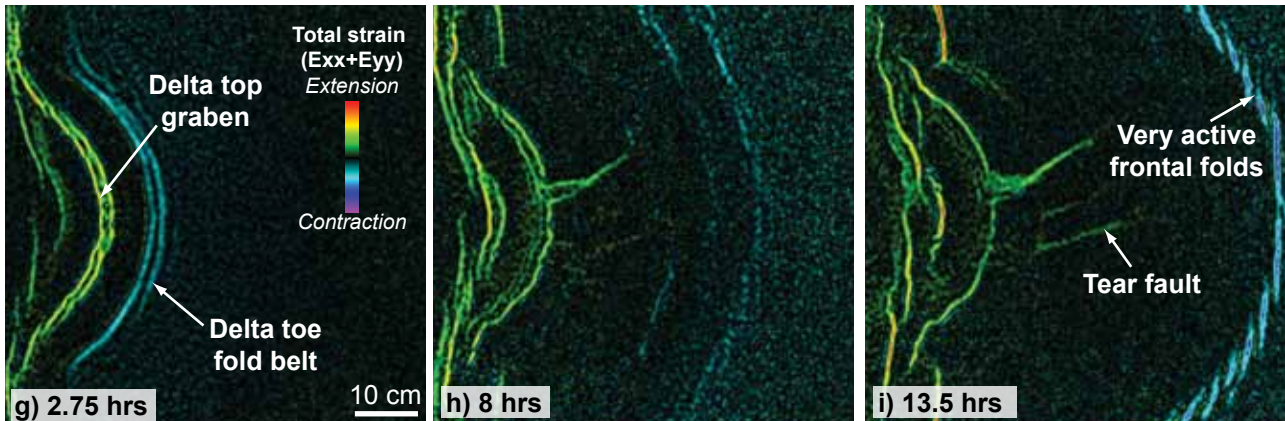
Interpreted structures



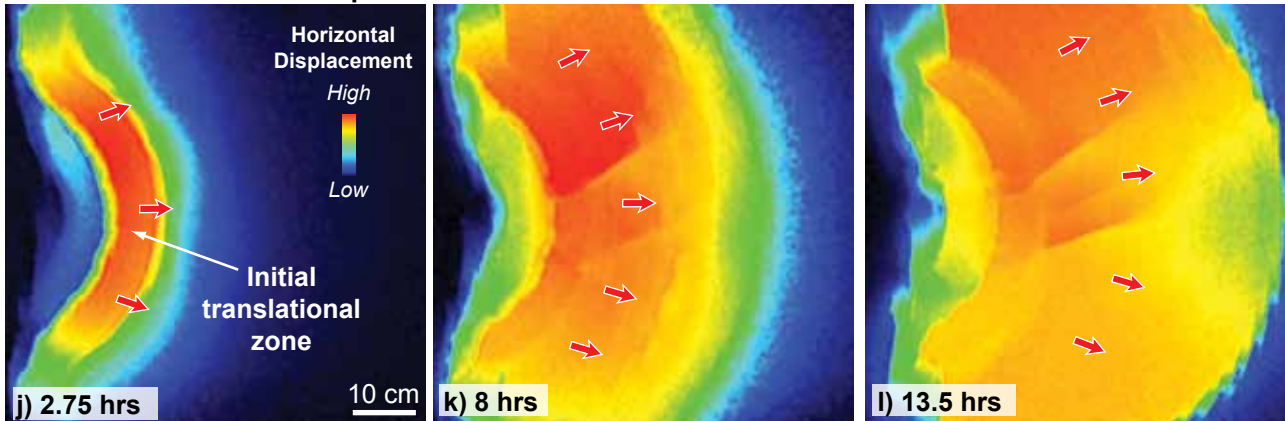
Incremental particle displacement vectors & top photograph



Incremental strain

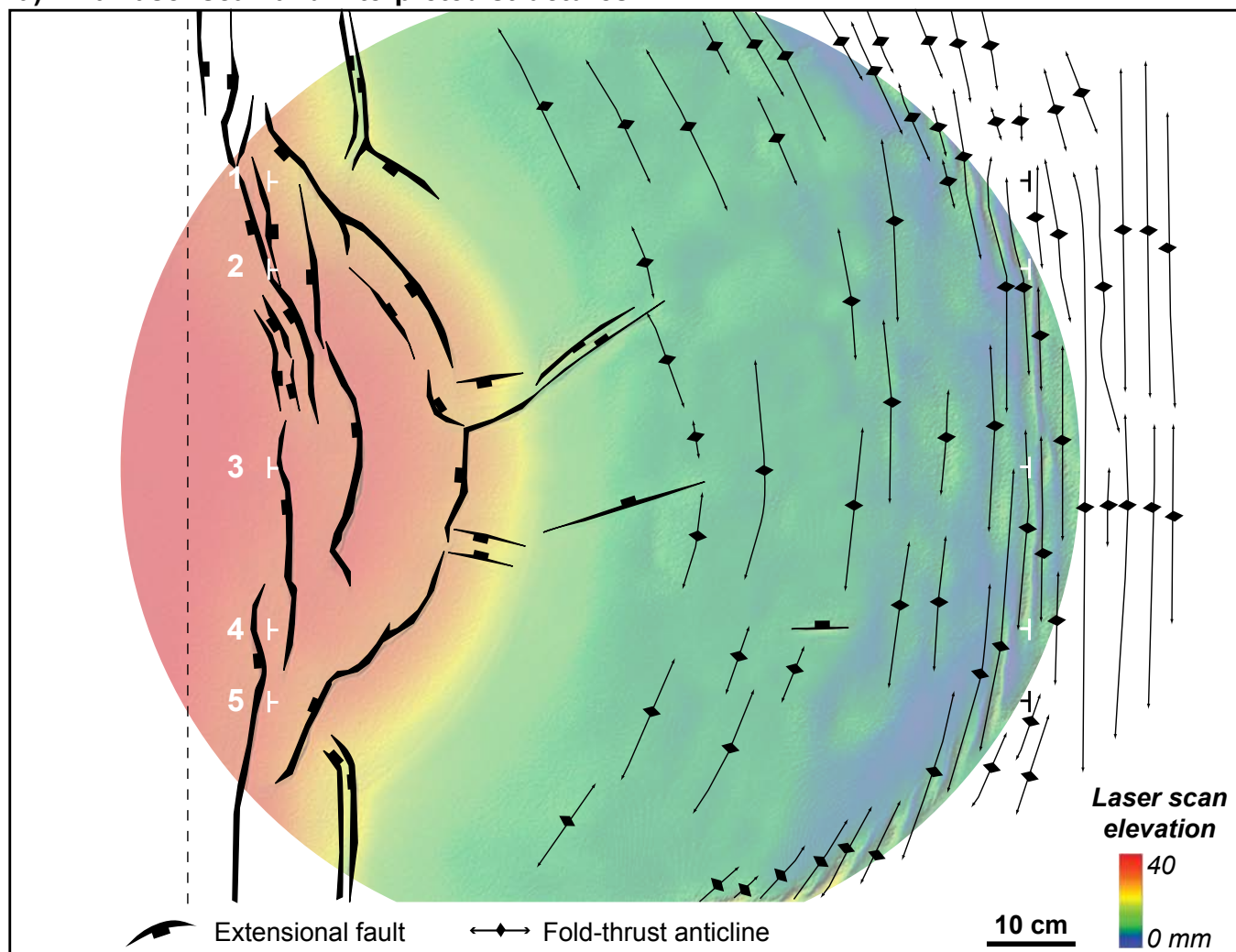


Incremental horizontal displacement

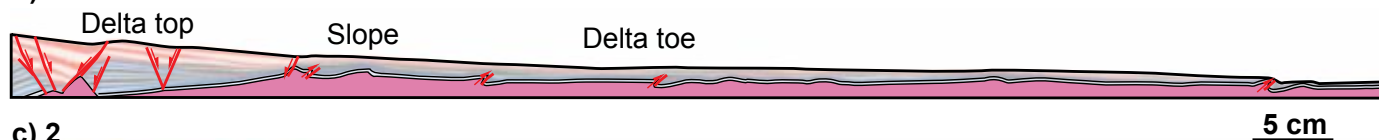


➡ Main gravity spreading directions

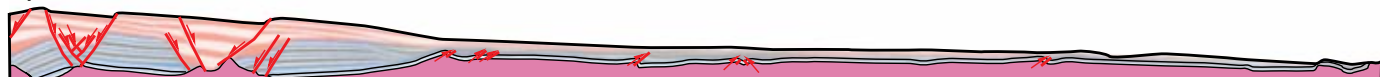
a) Final laser scan and interpreted structures



b) Section 1



c) 2



d) 3



e) 4



f) 5

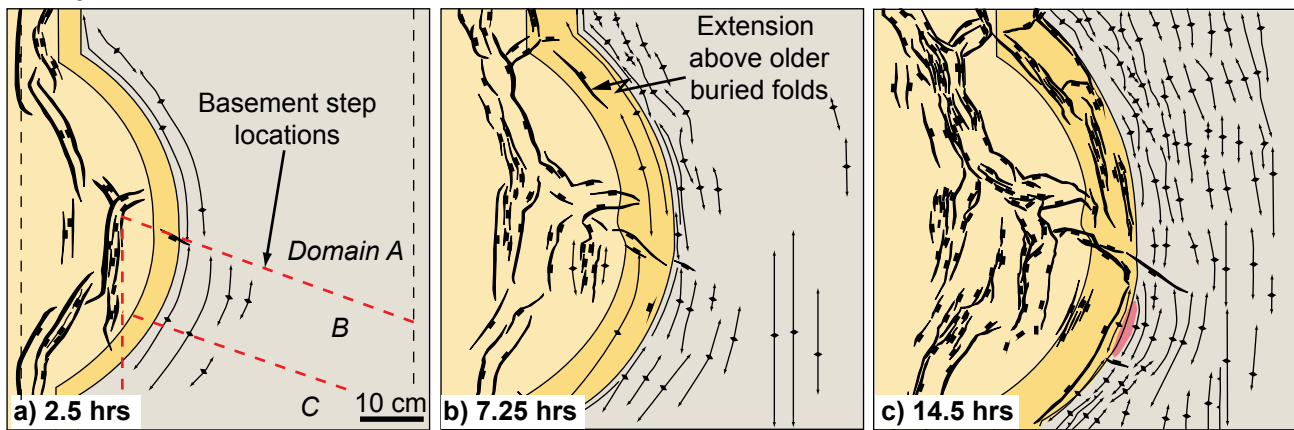


Syn-kinematic strata

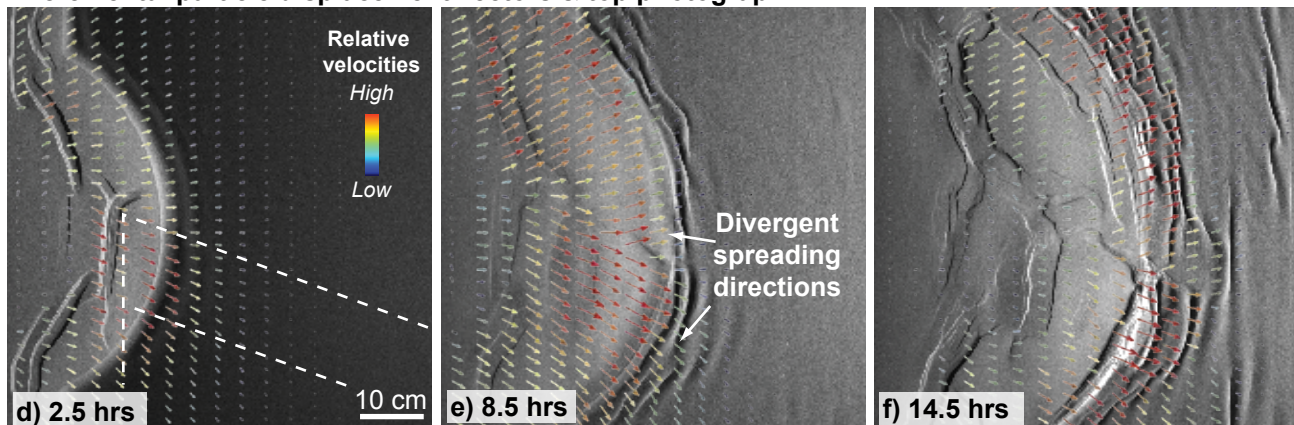
Pre-kinematic strata

Polymer

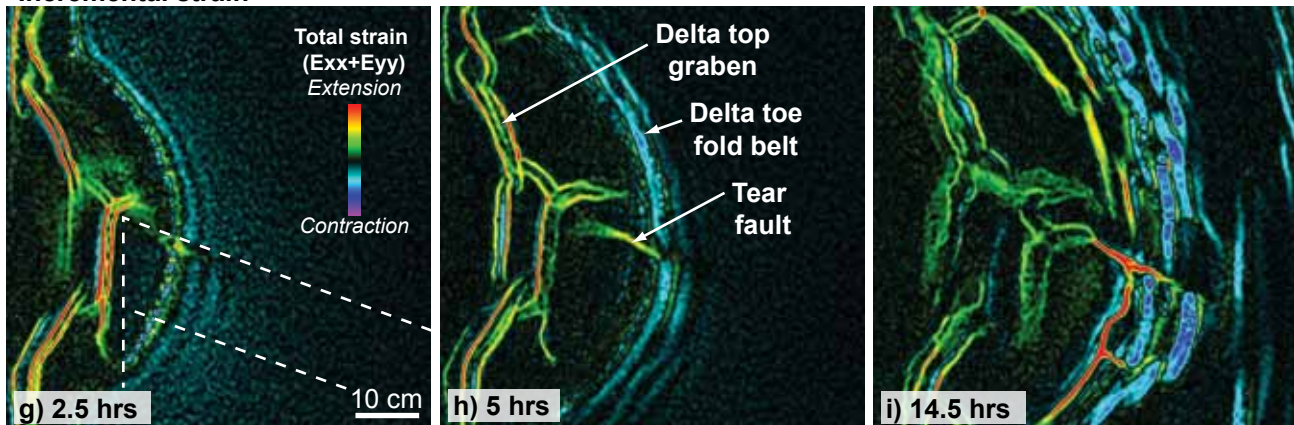
Interpreted structures



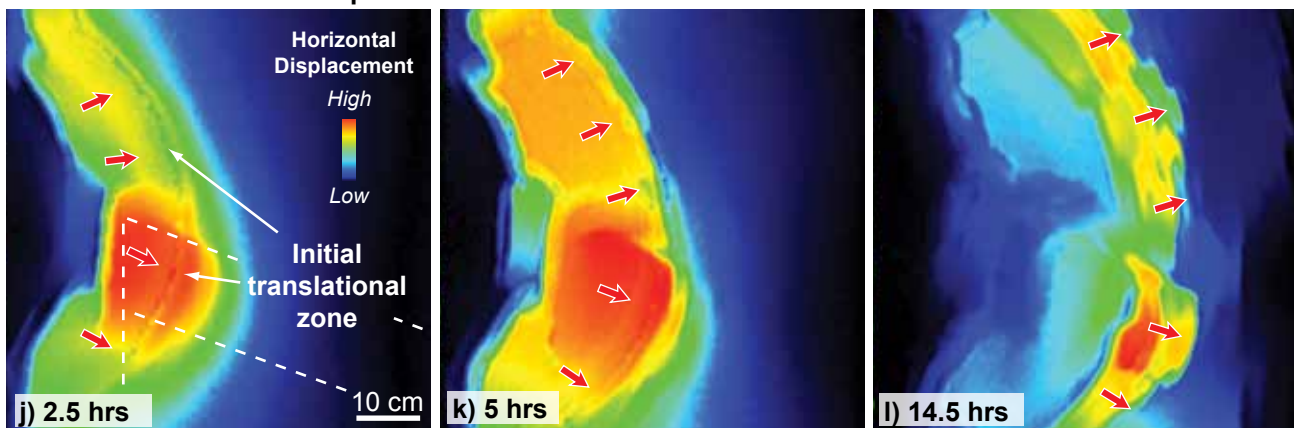
Incremental particle displacement vectors & top photograph



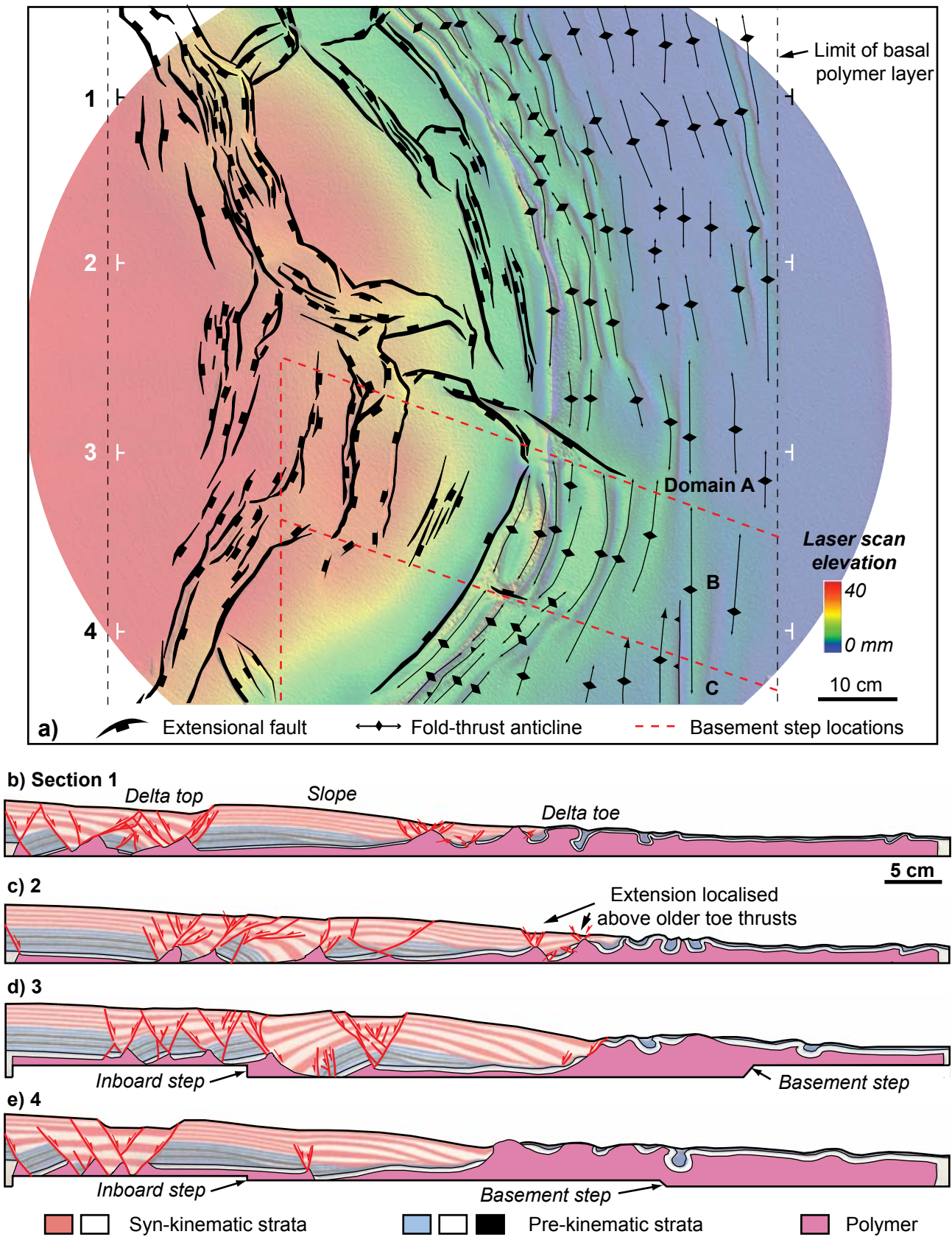
Incremental strain



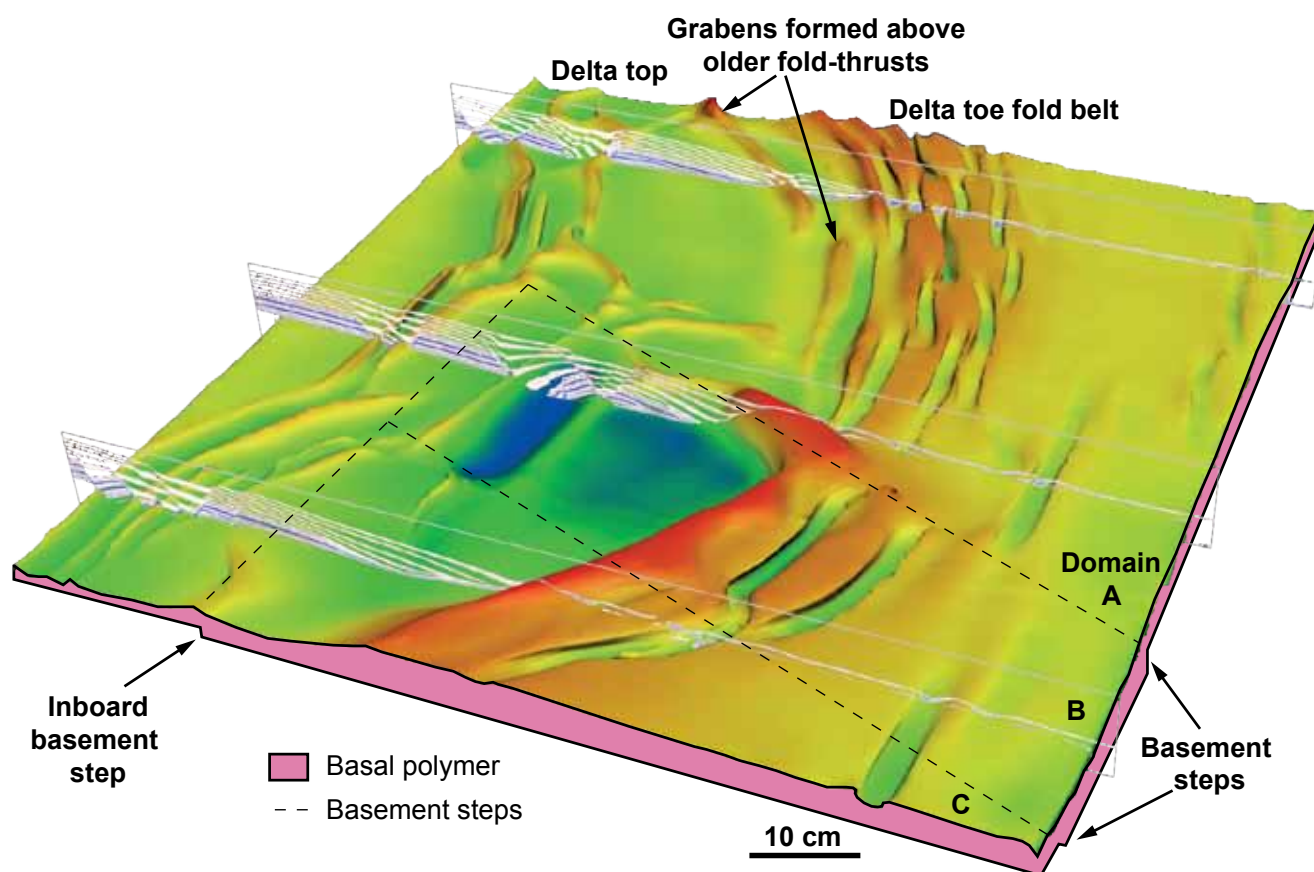
Incremental horizontal displacement



➔ Main gravity spreading directions

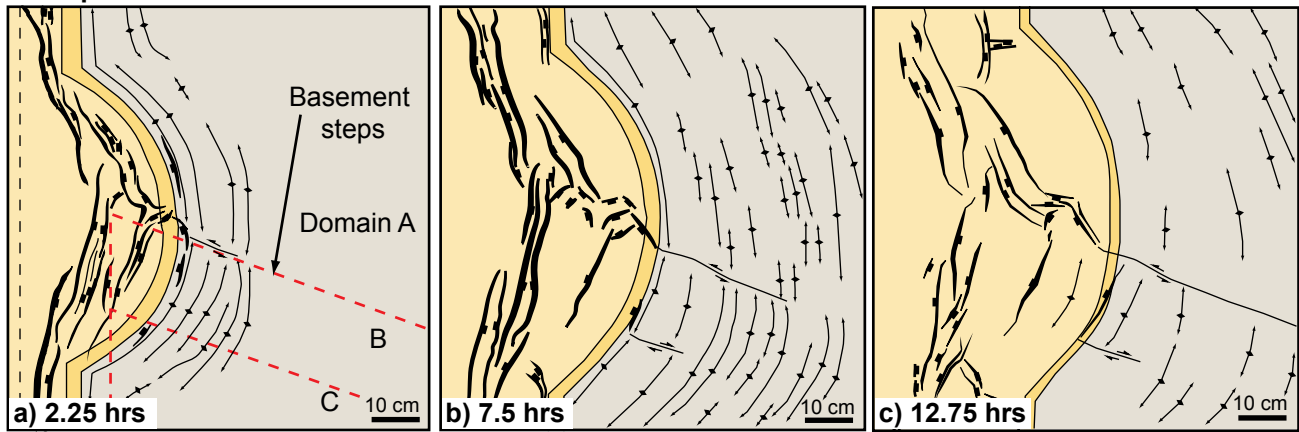


Wu et al. Figure 12

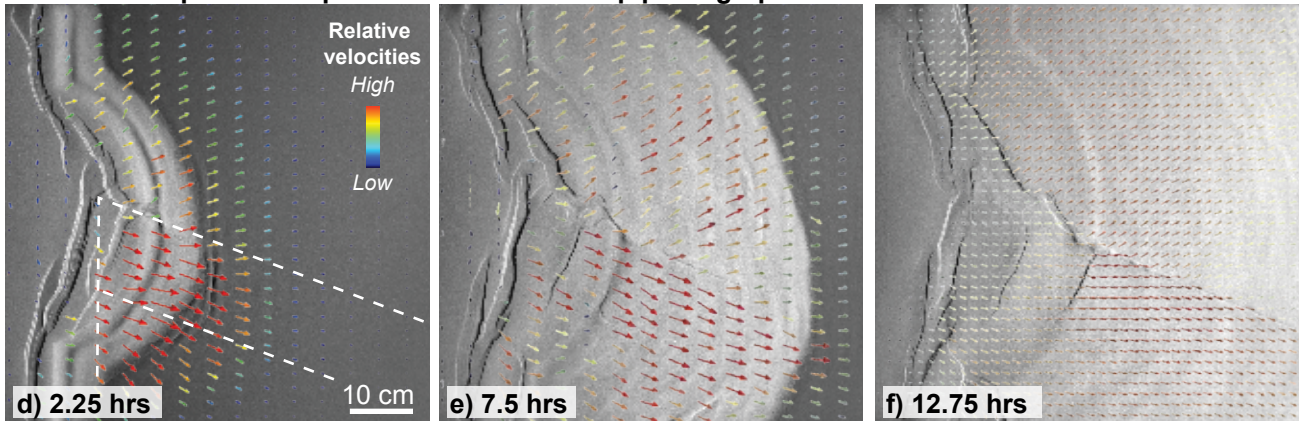


Wu et al. Figure 13

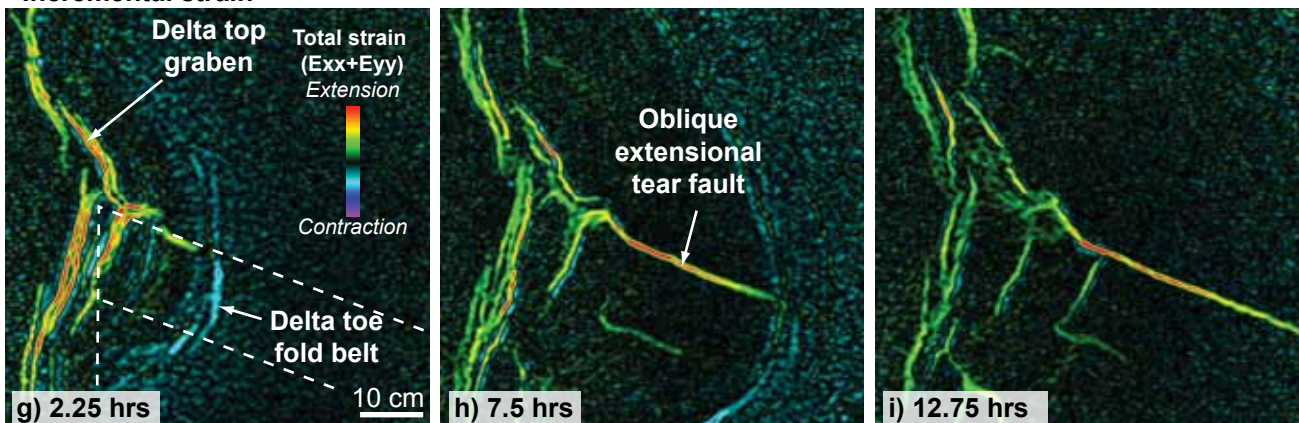
Interpreted structures



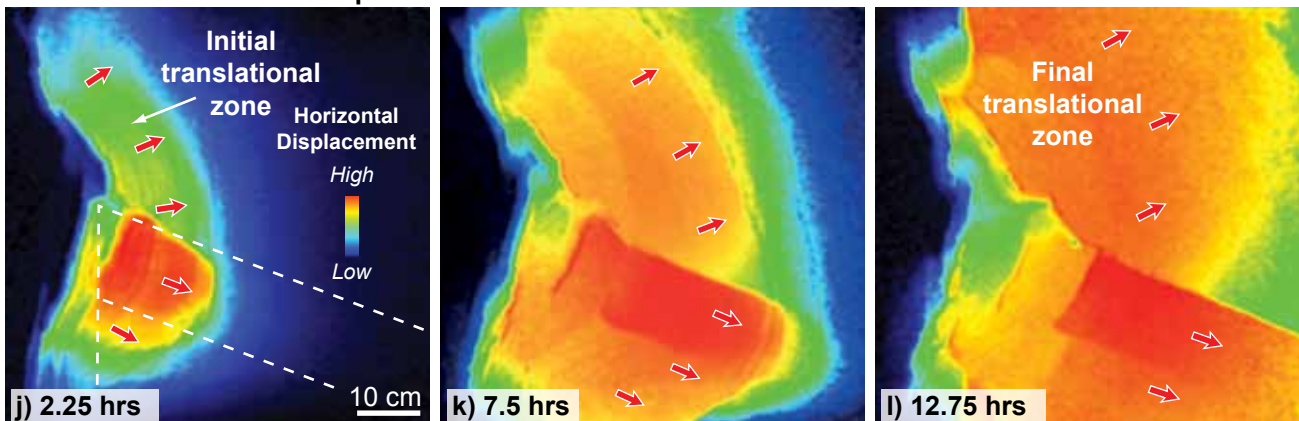
Incremental particle displacement vectors & top photograph



Incremental strain

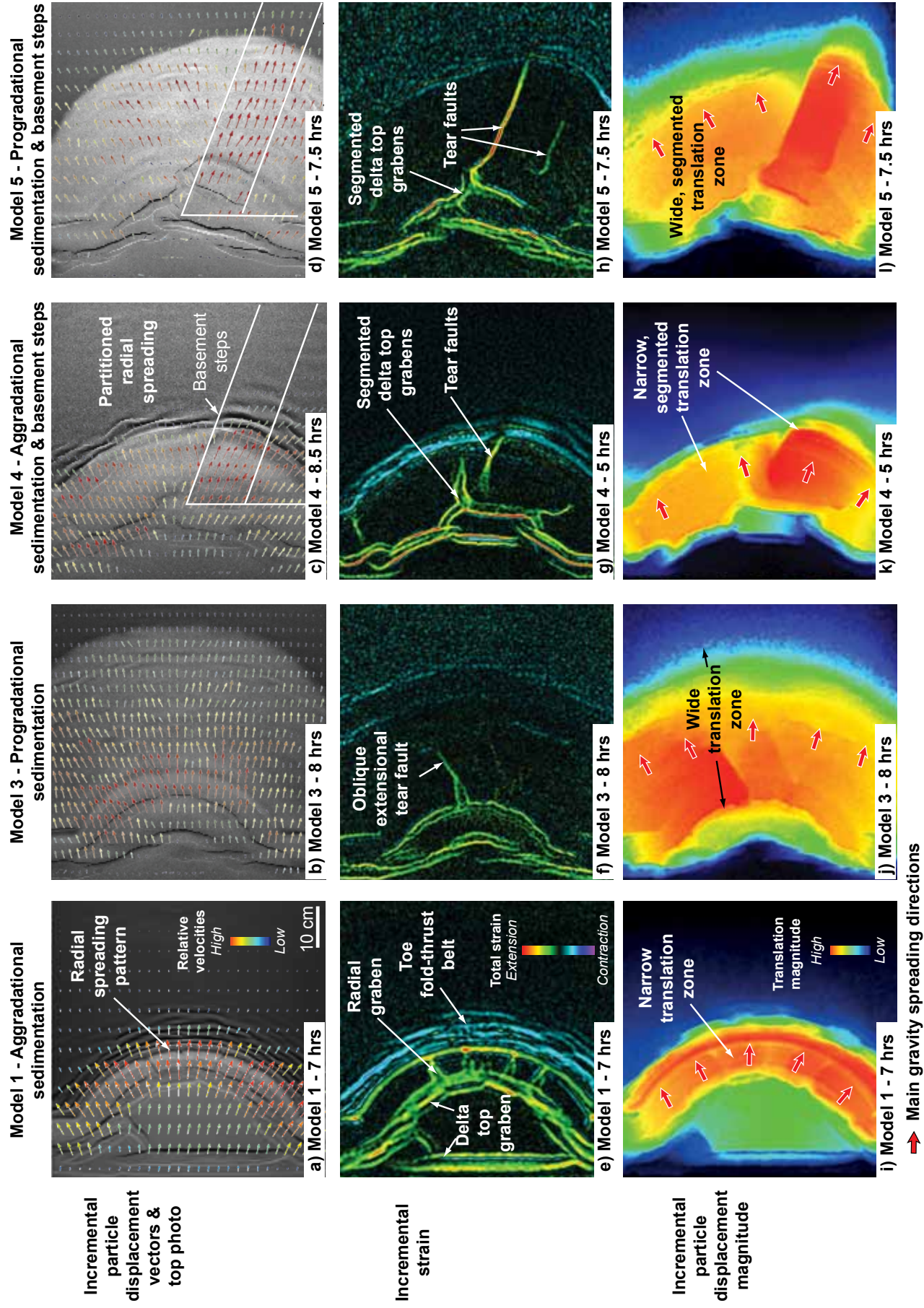


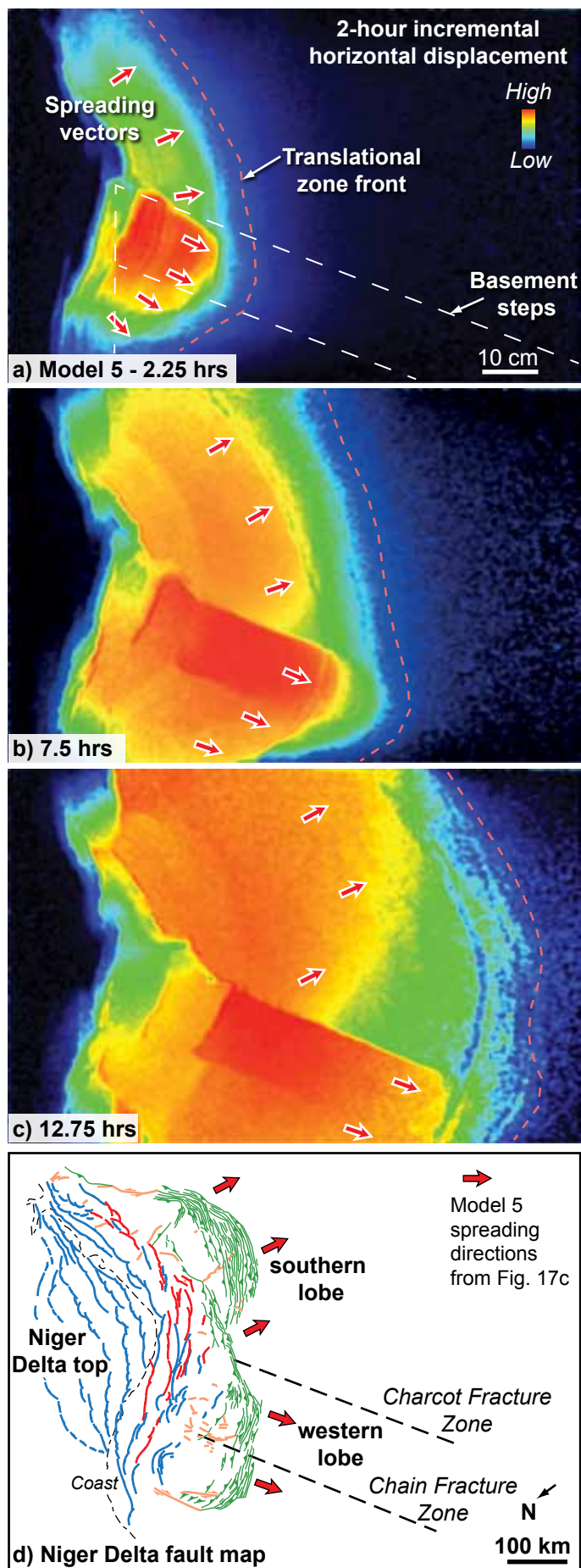
Incremental horizontal displacement



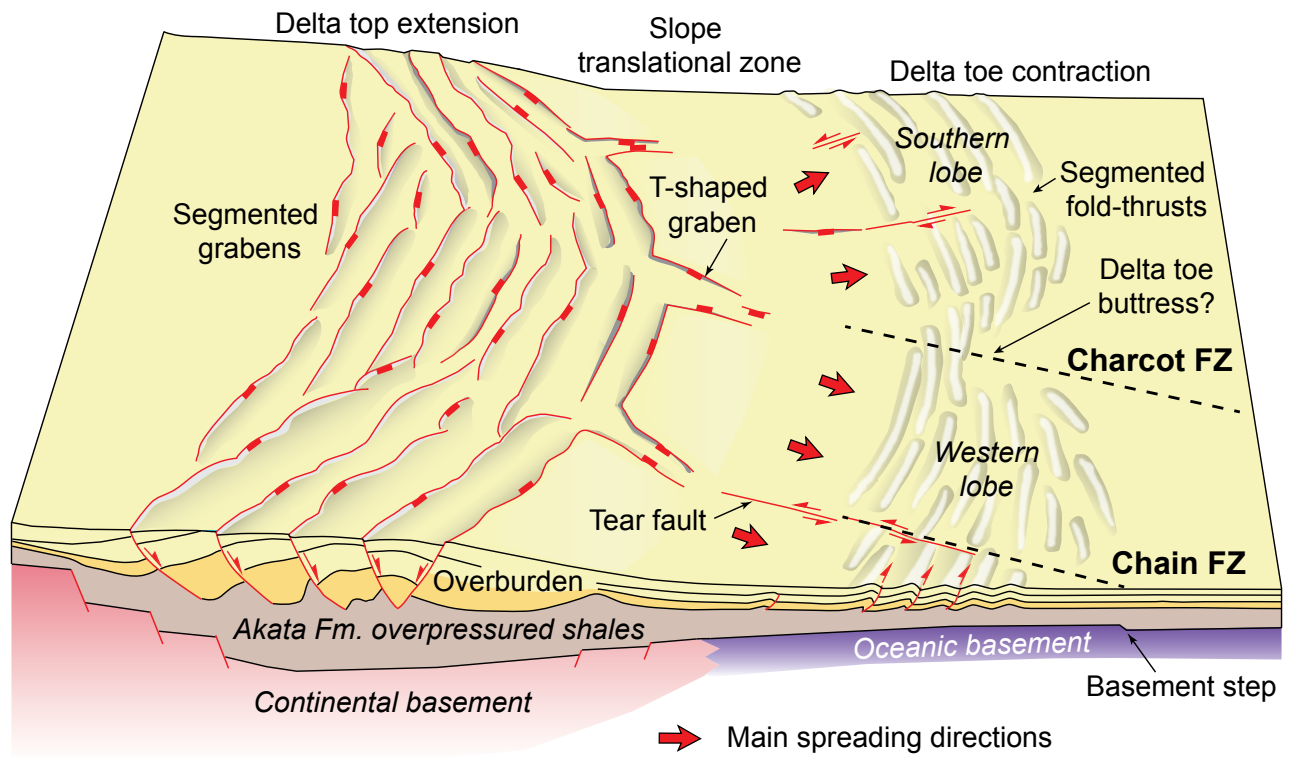
➔ Main gravity spreading directions







Wu et al. Figure 17



Wu et al. Figure 18

Model number	Model series	Syn-kinematic sedimentation	Basement topography	Basal polymer dimensions	Deformation time (hrs)
1	1	Aggradational	none	standard (80 x 100 cm)	13.5
2	1	Progradational	none	standard	13.5
3	2	Progradational*	none	double-length (158 x 100 cm)	11.5
4	2	Aggradational	basement steps	standard	14.5
5	2	Progradational	basement steps	double-length	12.75

Syn-kinematic sedimentation: *Aggradational - hourly sedimentation on delta top only*
Progradational - hourly sedimentation on delta top & delta toe fold belt
**additional thin 1mm sand layer between fold belt synclines applied between every 'progradational' event*

Wu et al. Table 1